The Pennsylvania State University

The Graduate School

John and Willie Leone Family Department of Energy and Mineral Engineering

EXPERIMENTAL INVESTIGATION OF EFFECTIVE MATRIX PERMEABILITY AND THE EFFECT OF SOAKING TIME IN ULTRA-TIGHT SHALES

A Thesis in

Energy and Mineral Engineering

by

Nirjhor Chakraborty

Submitted in Partial Fulfillment

of the Requirements

for the Degree of

Master of Science

December 2015

The thesis of Nirjhor Chakraborty was reviewed and approved* by the following:

Zuleima T. Karpyn

Associate Professor of Petroleum and Natural Gas Engineering
Quentin E. and Louise L. Wood Faculty Fellow in Petroleum and Natural Gas Engineering
Thesis Adviser

Luis F. Ayala H.

Professor of Petroleum and Natural Gas Engineering
Associate Department Head for Graduate Education

Sanjay Srinivasan

Professor of Energy and Mineral Engineering
John and Willie Leone Family Chair in Energy and Mineral Engineering

Shimin Liu

Assistant Professor of Energy and Mineral Engineering

Hamid Emami-Meybodi

Assistant Professor of Energy and Mineral Engineering

*Signatures are on file in the Graduate School

Abstract

Fluid flow behavior through ultra-tight shale matrices is still poorly understood. Applications of classical concepts to these unconventional materials are proving to be insufficient and there is a need to generate data on the fundamental processes of fluid transport through nano-porosity networks. This work attempts to address this issue through an array of flow and materials characterization experiments. The context of this integrated petrophysical analysis is the examination of the impact of fluid leakoff and post stimulation shut-in or "soaking time" on effective gas permeability. Past research on fluid leakoff and soaking time has been predominantly conducted with relatively high permeability rocks and for short durations of up to 15 days. We present data on shales with nano-Darcy (10^{-6} md) permeability and have run experiments for up to 30 days. A pulse-decay permeability apparatus has been custom designed to accurately measure gas permeabilities down to 1nD and the results have been scrutinized in conjunction with X-Ray CT, SEM imaging, Mercury Porosimetry and XRD analysis. Results indicate that laminations and micro-fractures play an important role in fluid transport properties in these ultra-tight shales. There appears to be very little connected porosity at scales longer than a few millimeters, making clastic permeability virtually non-existent. The consequences of fluid leakoff are severe and the introduction of relatively small quantities of liquid into the rock matrix leads to orders of magnitude reductions in effective permeability. The impact of this leakoff fluid then evolves significantly as it is spontaneously redistributed through the rock matrix due to capillary imbibition. Base permeability or the initial absolute (single phase) permeability of dry sample is found to be key to understanding the consequences of soaking time – high permeability samples experience relatively minor permeability impairment due to leakoff and permeability recovery with soaking time while tighter samples experience permeability damage greater than 90% due to

leakoff which continues to decline with soaking time. This raises the strong possibility that the practice of soaking in shale gas wells may be detrimental to long term production and ultimate recovery.

Table of Contents

List of Figures

List of Tables

List of Equations

Acknowledgements

I would like to dedicate this work to my parents and thank them for the innumerable sacrifices they've made for me to get to where I am today.

I'm immensely grateful to my adviser and mentor Dr. Zuleima Karpyn for her patience, support and guidance during this work. I couldn't have asked for more.

A very big thank you to Madhu Singh for the time she has spent with me in the lab, helping me with presentations of this work, and proof reading the thesis along with her artistic inputs related to the figures in this work. This work would not have been possible without her.

I also must thank Dr. Philip Halleck, Dr. Dustin Crandall and Timothy Stecko for the crucial technical help they provided at different stages of this work. The suggestions of my thesis defense committee members Dr. Sanjay Srinivasan, Dr. Shimin Liu and Dr. Hamid Emami-Meybodi have also been very valuable in improving the content of this thesis.

I must thank Dr. Luis Ayala for suggesting I work on this project with Dr. Karpyn in the first place. The faith shown in me by him and Dr. Karpyn is something truly valuable to me.

I would also like to thank my colleagues at the Center for Quantitative Imaging (CQI) Lab – Botros Abdelmalek, Samet Konya and Ugur Pakoz, and in the EME department – Sarath, Soumyadeep, Vaibhav and Putcha for their help and friendship. I've learned a lot from them and they've made work fun. They made the last two years a time that I shall forever cherish.

Last, but most importantly, I'd like to acknowledge my grandfather (Bapi Dadu). It's his faith, prayers and blessings that stay with me all the time.

1 Background

The fusion of horizontal well and hydraulic fracture technology in the early 2000s provided us the keys to unlocking the immense oil and gas resource that are shales. Shales now contribute over 40% of total US natural gas production and its share is expected to rise to 53% by 2040 **(EIA 2014)**. But despite this massive production boom, the idea of looking at shales as reservoir rock is still relatively new. In the past, petrophysical assessments of shales have been done to evaluate their efficacy as caps and seals **(Kastsube et al. 1991)** or to solve wellbore integrity issues **(Horsrud 1998)**. Today, we possess the tools to produce from these reservoirs but still have scant understanding of the fundamental physics of flow in these ultra-tight and nano-porous materials. A consequence of this is that today, on the order of one in three shale gas wells have poor production characteristics **(Kovscek 2015)**. A big opportunity therefore exists to improve the efficiency of stimulation treatments. A deeper understanding of the mechanical, petrophysical and fluid transport characteristics of shales will be an essential part of this endeavor.

Descriptions of shales along the lines of conventional reservoirs is fraught with inaccuracy. Conventional dual porosity-permeability models are insufficient to describe the complexity of fluid flow in shales and result in unreliable predictions of long-term production and estimates of ultimate recovery **(Cipolla et al. 2010)**. This is a consequence of a variety of factors that are unique to these reservoirs, such as, ultra-low matrix permeability (<100nd), mesoporosity (average pore size 20nm to 50nm), extensive laminations, complex fracture network, high clay content, gas adsorption etc. In recent years, several attempts have been made to build shale specific models that incorporate some of these differences such as inclusions of greater fracture density and complexity **(Cipolla et al. 2010, Gupta et al. 2013, Al-Obaidy et al. 2014).** While these new models undoubtedly offer improvements, there is general cognizance of the fact that simplified “one size

fits all" models continue to be inadequate in representing pore scale, local, field and basin scale heterogeneities in shale formations and indeed the significant differences between different types of shale.

In order to effectively understand the dynamics of fluid flow through shales, the first step is to develop an appreciation of the length scales we are looking at when dealing with tight rock matrices. At pore sizes of a few nanometers, surface effects stemming from rock-fluid interactions can become highly pronounced, relatively small pressure and fluid saturation changes can significantly alter permeable pathways, and Darcian flow principles almost cease to apply. In addition, fine particulate matter may be found near fractures existing in an almost fluidized state. **Glorioso and Rattia, 2012** noticed that measurements of common petrophysical properties such as porosity, permeability, saturation and lithology of the same (shale) rock type by different labs are notoriously disparate**.** This is, most probably, an expression of the heterogeneous nature of shales as well as a heightened sensitivity of these parameters to experimental conditions. Therefore, there is a need to fundamentally re-evaluate the way in which we analyze and characterize these formations. Additional tests such as X-Ray Diffraction and X-Ray Fluoroscopy for assessing composition, centrifugation for grain size, Mercury Injection Porosimetry (MIP) for bulk porosity and pore size distribution, SEM for porosity characterization and X-Ray CT for macro scale fracture connectivity are becoming the new staple for complete characterization of shales **(Josh et al. 2012).**

While a lot has been said about the diversity of shales, modern characterization techniques are also revealing certain common threads across different plays (**Schieber 2010, Curtis et al. 2010)**. Detailed SEM analysis of 6 different shales by **Schieber 2010** revealed that porosity could be classified into 3 broad categories – Phyllosilicate framework (PF) pores existing within clay

particles and ranging from 5nm to 1μm, carbonate dissolution (CD) pores ranging from 50nm to 1μm, and organic matter (OM) pores ranging from 10nm to 100nm. When analyzed in conjunction with measurements of total organic content (TOC) a trend that emerged was that rocks with high TOC (>10%) tended to have PF pore space filled in with kerogen/bitumen, whereas, rocks with low TOC (<7%) tended to have more open and connected PF pores that could potentially serve as gas flow path ways. CD pores, on the other hand, tended to be large but isolated when carbonate content was low. However, in shales, with a large proportion of carbonates, these pores tended to concentrate into extended laminae that could serve as significant permeability channels. These insights from pore scale characterization might very well explain observations by **Britt and Schoeffler, 2009** that the most productive shale plays tended to be composed of large amounts of silica and carbonate and were usually brittle. Contemporaneous but independent SEM studies by **Curtis et al. 2010** on 9 different shale formations also similarly documented porosity to fall into three categories – crack like, organophyllic and phyllosilicate porosity. Still, very little (experimental) literature exists that attempts to correlate sub-micron level observations with intermediate and macro scale properties.

The fact that the petrophysical properties of shales are scale dependent has been known for a while **(e.g. Neuzil 1994).** It is commonly believed that the productivity of a shale gas well is controlled primarily by hydraulic and large transmissive natural fractures and therefore, there has been a lot of research on fracture conductivities **(Cuisat et al. 2002, Olson et al. 2014, Zhang et al. 2014).** Matrix permeability, on the other hand, has been considered secondary and most applications assume one homogenous value for large portions of the reservoir. This simplification could be quite dangerous for shale formations. **Heller and Zoback, 2014** found that shale permeability measured on 1inch diameter and 1.5 inch long cores was higher by 1 to 2 orders of magnitude than

measurements made on crushed samples. This is an indication that a simple conventional clastic rock like imagining of the fluid flow network might be incorrect for shale matrices. At intermediate scales such as core plugs, features such as cracks and micro-fractures **(Heller and Zoback, 2014, Tinni et. al. 2012)** or relatively high porosity-permeability cementation channels **(Vega and Kovscek 2013, Landry et al. 2014)** might enable shales to mimic conventional reservoir rock characteristics such as capillary imbibition whereas, in reality, most of the matrix looks very different. Currently the most widely used procedure for evaluating tight matrix permeability is the Gas Research Institute (GRI) method of permeability measurement on crushed samples which cannot account for such features. It is therefore also impossible to use this approach to measure two-phase effective matrix permeability in very tight rocks and there is currently no accepted protocol for such experimental measurements.

Several authors have claimed, on the basis of simulation models, that time dependent damage to fracture face permeabilities has very little effect on long term productivity of shale gas wells **(Holditch 1979, Li et al. 2013, Cho et al. 2013)**. However, this has not been backed up by experimental evidence yet. These simulations are based on conventional models of homogenous and uniformly distributed porosity and permeability of the rock matrix, and are therefore vulnerable to underestimations of damage caused by effects such as increasing effective stresses and fracture fluid leakoff. After extensive simulation tests, **Holditch 1979** concluded that only when the fracture-face permeability damage is greater than 99% will there be any significant productivity impairment in conventional gas wells. **Li et al. 2012** set this damage threshold at 95% for shale wells. Both **Holditch 1979** and **Li et al. 2012** are of the opinion that this level of damage is unlikely to be caused by fracture fluid leak off, and **Cho et al. 2013** suggest that damage from

fracture closure due to real stresses will not exceed 80%. The only way to verify these claims is to conduct experiments on representative samples of the rock matrix.

In recent years, theoretical and experimental studies on the factors damaging productivity of hydraulically fractured shale gas wells **(Bahrami et al. 2011, Pagels et al. 2013)** are converging to the broad conclusion that the large quantities of water based fracture fluids left unrecovered at the start of production cause permeability damage and productivity impairment. These volumes of fluid lost to the reservoir are, on an average, over 75% of the injected volume and, in some extreme cases, as high as 97% **(Lan et al. 2014)**. This fracturing fluid may initially occupy a large proportion of the fracture volume thus "clogging-up" the high permeability flow channels. This may explain the low productivity reported by operators when wells are put on production immediately after stimulation. With time this fluid is thought to spontaneously imbibe into the rock matrix due to the very high capillary pressures that exist in tight rocks **(Holditch 1979, Roychaudhuri 2011, Dutta et al. 2014)**. This leads to the clearing up of clogged fracture channels, significantly improving connectivity with the reservoir, leading to higher productivity. Therefore, providing "soaking time" or shutting in of wells for some time after stimulation has become a widespread practice. However, soaking time can also have negative consequences arising out of the formation of liquid blocks in the near fracture region. This skin-like damaged zone tracing the surface of fracture network can potentially hamper both long term productivity and ultimate recovery. There is still very little data on which of these two opposing factors is more important and therefore selection of the duration of soaking time is still arbitrary among most operators and ranges from as little a week to as much as a year. This work attempts to bring more clarity to the issue by consolidating literature on fluid leakoff and soaking time, mostly available for high

permeability rocks, and conducting experiments to fill in some void remaining in terms of ultra-low permeability rocks.

Some recent studies have shown that the permeability in tight rocks can fall by 50% to 90% due to the presence of liquid blocks **(Odumabo 2014, Bostrom et al. 2014, Yan et al. 2015)**. Indications are that this permeability damage can be reversed to a certain extent by prolonging the shut in time **(Odumabo et al. 2014, Bostrom et al. 2014)**. During this additional shut in period, it is believed that, capillary forces continue to act on the fluid in the invaded zone, redistributing it from a localized high water saturation volume into a larger volume of lower water saturation propagating deeper into the matrix. In conventional and tight sands, this lowering of water saturation is what leads to the recovery of effective permeability **(Odumabo et al. 2014)**. These results of milli-darcy permeability rocks may not apply equally to tighter shale matrices. The growth of the fluid invaded zone can have a detrimental effect on shales due effects such as clay swelling **(Yan et al. 2015)** and the existence of high critical gas saturations. The work by **Yan et al.** provides some insight into the consequences of soaking time on shales through experiments on 10-20μD ranged Haynesville shale samples. However, many of the prolific shale reservoirs are ultra-tight with nano-Darcy permeability for which soaking time experiments have not yet been reported in literature. In addition, the experiments by **Yan et al.** were limited to 14 days. There is no data in literature on the rates at which leakoff fluid spontaneously spreads through ultra-tight matrices and it might therefore be useful to extend the time frame of soaking time experiments, which is what has been done in this work, for up to 30 days.

A highly sensitive pulse decay setup **(Jones 1997)** has been used to accurately measure the permeability of Haynesville and Marcellus shale core plugs with single phase permeability of around 100nD and two-phase permeability as low as 1nD. Brine is injected at one face of the core plugs to simulate the initial fracture fluid invasion and the formation of near fracture liquid blocks. Thereafter, all external pressure gradients are removed to allow the brine to spontaneously propagate under capillary forces alone whilst the countercurrent gas phase permeability is periodically measured. A series of additional tests are also done to understand the pore scale properties of the rock. These include micro-CT scanning, SEM imaging, X-Ray Diffraction, and Mercury Intrusion Porosimetry (MIP). The results of this integrated petrophysical analysis is combined with data from other soaking time experiments found in literature in order to provide a broader understanding of its consequences across a range of lithologies.

2 Research Objectives

Based on a review of literature on the current state of knowledge on the petrophysical properties of partially water saturated shale matrices, the main objectives of this work have been formulated as follows:

1. To develop an effective protocol for measuring two-phase permeability in ultra-tight porous material.

   Currently the industry standard for measuring matrix permeability in very tight rocks is the Gas Research Institute (GRI) method of using crushed rock samples. This approach cannot account for matrix permeability anisotropy and important features such as cracks, micro-channels such as fractures, vugs and laminations. It also precludes measurements of two-phase effective and relative permeability. There is currently no experimental protocol for relative permeability measurements in shales and therefore we are forced to rely on pore scale simulation models (**Cantisano et al. 2013, Daigle et al. 2015**) to generate this critical data. An alternate experimental approach is to use pulse-decay techniques which can be used for core plugs. However, the most recently proposed pulse decay protocol by **Jones, 1997** was only applicable and practical for rock permeability as low as 1μD. A modified experimental setup and measurement protocol is therefore required to quickly and accurately measure two-phase gas permeability down to 1nD.

2. To experimentally evaluate the impact of fluid leakoff on matrix permeability in ultra-tight shales.

   This is an extension of similar experiments reported in literature for rocks with permeability higher than 1μD. This work specifically focuses on rocks which have a single phase gas matrix

permeability of less than 200nD. This will provide an insight of the consequences of fluid introduction into the near-fracture matrix of ultra-tight shales during hydraulic fracturing.

3. To experimentally investigate the evolution of effective two-phase permeability with time in ultra-tight shales.

   Although post-stimulation shut-in time is a common practice in the development of shale gas reservoirs, there is almost no literature in clear support of this practice. While there have been some studies that demonstrate the possible benefits of this practice in less tight reservoirs, the damage caused by leakoff is more severe in ultra-tight rocks and soaking time may further exacerbate this problem. There are no experimental studies reported in literature on the consequences of soaking time on ultra-tight matrices during the time scale of well shut-ins which are on average around 30 days. This experimental work carried out in this study attempts to fill that void.

3 Experimental Methodology

3.1 Soaking Time Experiments

Soaking time experiments were designed to study the permeability of the near fracture matrix during the post stimulation shut-in period. During this period the effective permeability of the rock matrix continuously changes due to redistribution of leakoff fluid driven by capillary forces. This process is illustrated in **figure 3.1**.

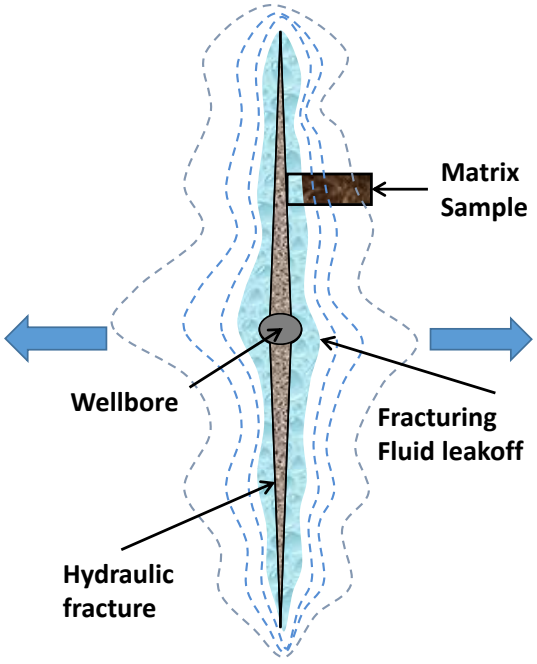

Figure 3.1: Artist rendering of fluid leakoff and capillary imbibition in the matrix region around a fracture. The core plugs used for lab measurement are a sample of un-fractured reservoir rock matrix. Adapted from Dutta et al. 2014.

Field scale tests, such as repeat formation tests (RFT) and well test analyses, cannot be used to measure the pre-stimulation permeability of shale reservoirs. But in the lab, it is possible to dry out core samples and therefore, as the first step, establish a base permeability value of clean rock. Controlled volumes of fluid injected at pressure gradients of around 13.8 MPa (2000psi), which is typically the extent to which injection pressures exceed pore pressure in real hydraulic fracturing

operations, represent fluid leakoff. This injected leakoff fluid, subsequently allowed to spontaneously spread into the rock under capillary forces, mimics soaking time. The permeability to gas in the counter-current direction to liquid movement, periodically measured, represents the flowback permeability.

3.1.1 Sample Preparation

Samples of Marcellus and Haynesville rock were extracted from slabbed well cores of 2.75cm (1.5") radius. Most of these cores were heavily fractured as can be seen from **figure 3.2**. The fracture spacing was around 2 to 6 cm. The made it challenging to core plugs of 2.5cm (1") diameter that were required for permeability tests. In addition sample were prone to fracturing along laminations during the coring process as well. In order to provide mechanical stability to the sample, the sections of the well cores were cased in epoxy as shown in **figure 3.3**. The dimensions of the samples finally cored and used for permeability measurements are given in **Table 3.1.** All samples were heated in an oven for 24 hours in order to dry out any water that might have been introduced during the coring process. The variance in the lengths of the samples was mostly a result of breakages along laminations during the coring process. This necessitated the paring of samples to maintain their cylindrical shape.

Table 3-1: Orientation relative to laminations and dimensions of samples used for permeability and flow experiments

Rock Type	Sample	Orientation	Diameter (inch)	Length, cm (inch)
Marcellus	M1	Parallel	1"	6.25 (2.5")
	M2	Parallel		4.75 (1.9")
	M3	Perpendicular		1.75 (0.7")
	M4	Perpendicular		0.20 (0.08")
Haynesville	M3	Parallel		4.50 (1.8")

Figure 3.2: Slabbed Marcellus core - 3.8cm (1.5") diameter and 3cm in length showing multiple parallel to lamination fractures spaced 2-3cm apart

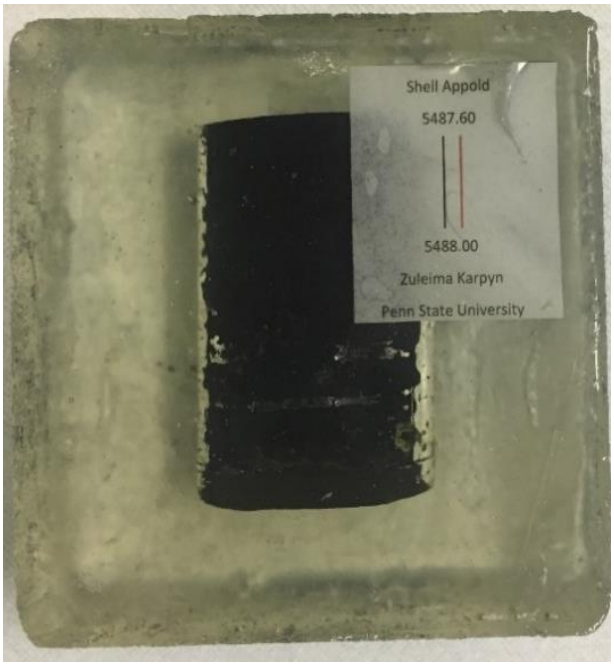

Figure 3.3: Well core cased in epoxy resin to provide mechanical stability during the coring process

3.1.2 Procedure

Experimental Procedure

The experimental procedure is outlined in **figure 3.4.**

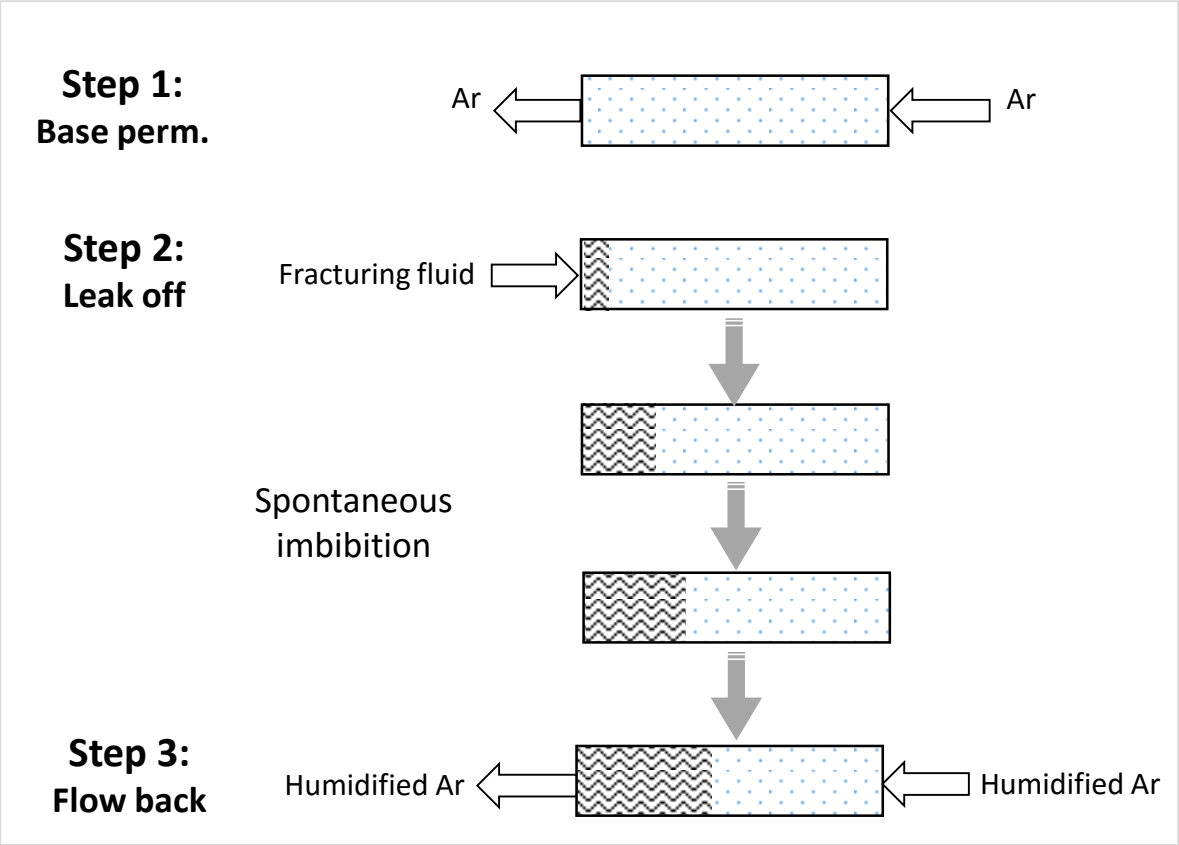

Figure 3.4: Experimental procedure for soaking time experiments

1. The first step of the process was to measure the permeability of the dry core plug in order to establish a baseline permeability to gas.
2. Next, brine was injected at high pressure gradients for several hours in order to emulate fluid leakoff at the fracture matrix interface. The brine solution used for this purpose was injected from the downstream end of the sample. This is because in a real reservoir the direction of entry of fracture fluid would be opposite to the direction of gas flow during production.
3. After the establishment of a liquid block, injection was stopped and there were no further pressure gradients applied across the two ends of the sample to force liquid flow. This

allowed for all subsequent imbibition and redistribution of the liquid brine to be spontaneous.

4. Gas permeability measurements were taken periodically at intervals of around 24 hours.

3.1.3 Fluids

A 5% by weight Potassium Iodide (KI) brine was used as leakoff fluid.

Argon was chosen as flowback gas. This was done for three reasons – as a noble gas, argon was a safer option than natural gas; adsorption effects could be neglected; and being a larger molecule than Helium, the risk of leakage through the core plug jacketing could be reduced. To minimize water transfer of the leakoff brine into the gas phase during gas permeability measurements, argon was passed through a humidifier before being allowed to flow through the sample.

3.1.4 Apparatus

To measure effective gas permeability on the order of a few tens of nano-Darcies in reasonable time frames, a pulse-decay approach was adopted. For this purpose, a modified version of **Jones 1997** was custom built (**figure 3.5**). A pulse-decay approach works on the basic principle that when a small gas pressure differential is applied across the two ends of a core plug sample, the rate of gas diffusion through the rock plug reflects in the rate at which the upstream and downstream pressures equilibrate, and this data can be used to compute the permeability of the sample. A key parameter controlling the speed of measurements is the ratio of the upstream and downstream pressure application volumes (V_1 and V_2) to the pore volume (V_p). The fastest measurements occur when these ratios are close to 1. Since shales have very low porosity, V_p was often just a few milliliters. Therefore, V_1 and V_2 were just the volume of the flowlines between the

upstream and downstream valves. A second parameter that contributes to faster and more accurate pulse-decay measurements is high mean gas flowing pressure (**Jones, 1997)**. Thus, a mean gas pressure of 6.9MPa (1000 psia) was chosen, which was applied at the beginning of every permeability test using volumes V_3 and V_4, until static equilibrium was attained. This mean pressure was maintained during gas flow as well by setting up the pressure pulse with upstream pressure of 7.6MPa (1100 psia) at V_1 and downstream pressure of 6.2MPa (900 psia) at V_2. Upon establishment of this pressure gradient or "pulse", valves X_1 and X_{21} were closed, thus forcing gas to flow through the core sample only.

Argon becomes supercritical at pressures above 4.9MPa (715 psia) at room temperature. Therefore, the flowing properties of the gas such as viscosity, density and compressibility could be considered uniform throughout the experiment. The measurements of the upstream and downstream pressures were done using Quartzdyne DSB-301-10-C85 transducers with pressure sensitivity down to 0.01psi.

The rock samples were jacketed using polyolefin heat shrink tubing and a hydraulic confining pressure was applied around the jacket. A major challenge in this experiment was that the low permeability of the shales made them vulnerable to gas bypass between the sides of the core plug and the jacketing, which could result in gross overestimations of permeability. In order to minimize this gas bypass, the confining pressure was set at 16.5 MPa (2400 psia), which is twice the maximum gas pressure (7.6 MPa in the upstream). This had the added advantage of closing some of the micro fractures in the rock formed during the coring process. This core holder assembly

formed the heart of the pulse decay permeability setup. Its assembly process has been shown in **appendix 7.1**.

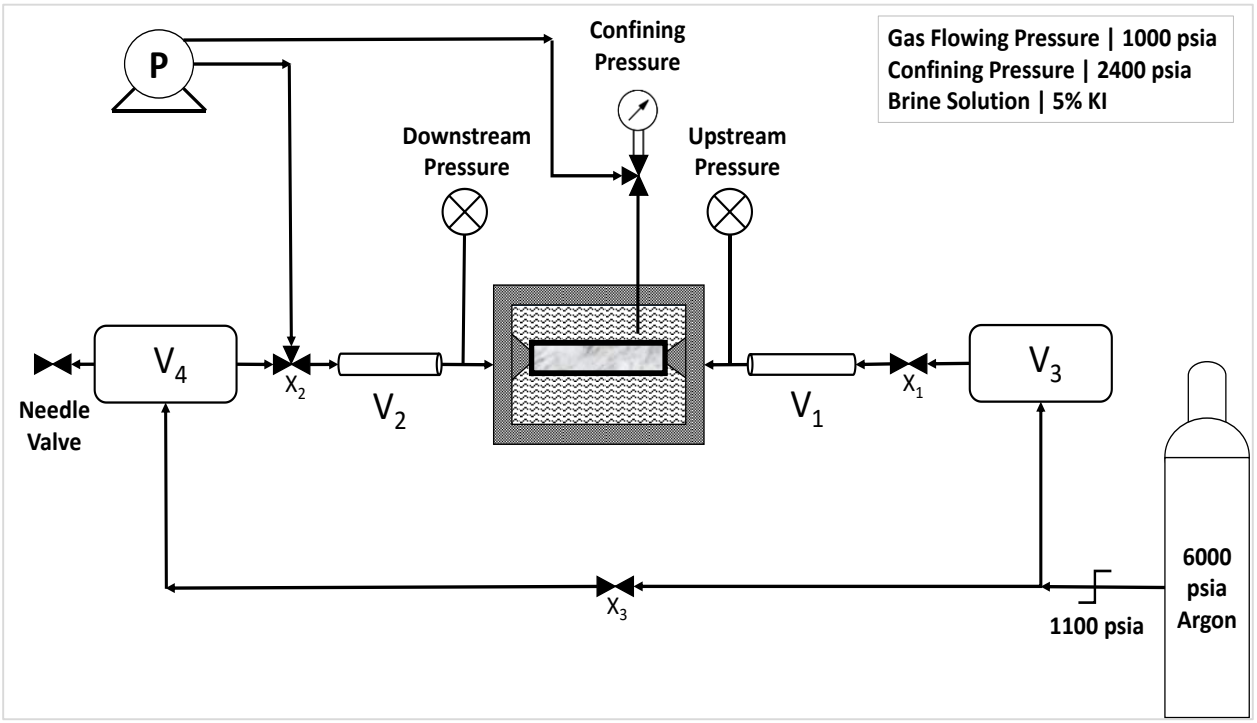

Figure 3.5: Schematic of pulse decay permeability measurement setup

The time frame of pulse decay measurements is highly sensitive to the average permeability of the samples. The time taken for pressure pulse equilibration was typically only 2 hours for permeability measurements of around 100 nD and greater than 72 hours for permeabilities of less than 10 nD. The time scale of measurements at these levels was on the order of several days. For measurements that ran into several days, permeability calculation was done based on the initial 24-hour straight-line slope of the pressure decay versus time semi-log graph. The conversion of this data to permeability has been done using the following equation from **Jones 1997**:

$$k_g = \frac{-14696 m_1 \mu_g L f_z}{f_1 A p_m * \left(\frac{1}{V_1} + \frac{1}{V_2}\right)}$$

Equation 3-1

The process of converting pressure data to permeability has been described in detail **appendix B**.

In order to maintain accuracy of measurements, the gas leakages had to be minimized. An impermeable synthetic core sample was fabricated using stainless steel in order to evaluate leakages. The gas leakage rate of the apparatus was maintained below 0.01%/day or 0.69kPa/day (0.1psia/day) at a mean gas pressure of 6.9MPa (1000psia). The limit of precision for the permeameter was estimated at 1nD. The errors in measurement were estimated through multiple base permeability readings on each sample. The maximum deviation of 2000 nD (2μD) from mean was observed in the fractured Marcellus M2 sample. However, the maximum percentage deviation of 15% from mean was observed with the Haynesville H1 sample. It was observed that a percentage based method of characterizing the errors were more accurate than an absolute value. Therefore, including a safety factor, the maximum expected is around 20%.

Water was used as confining fluid and was injected using a Quizix SSP-5200 pump. The same pump was also used later on in the experiment to introduce leakoff fluid into the sample. This injection was done at 10Mpa (1500 psia) at the downstream end of the core sample, with the upstream end at atmospheric pressure. The injection duration varied depending on the pore volume of the of the core sample, since the goal was the introduction a small liquid average saturation, with most of this liquid concentrated at one end. Injection durations were 4 hours for sample H1,

12 hours for M1 and 1 hour for M2. It is unclear how much liquid was actually injected into the samples. Weight measurements before and after the experiment were attempted in order to measure actual saturations. However, damage to samples during post experiment extraction from the jacketing made it inaccurate to attribute weight changes to fluid introduction. Based on the applied injection pressure, measured permeability and injection duration, the injected average liquid volumes have been calculated using Darcian flowrate multiplied by the injection time.

$$V_{injected} = q\Delta t = \frac{k}{\mu}\left(\frac{\Delta P}{L}\right)\Delta t$$

Saturations ($V_{injected}/V_p$) are estimated to have been between 7 and 20%. The biggest source of error in this calculation is the use of measured gas permeability ($k = k_g$) to liquid flow at 100% gas saturation.

In order to verify the results obtained by the pulse decay permeameter, single phase steady state flow experiments were also conducted to measure absolute permeability. These experiments can take extremely long for ultra-tight samples. To minimize the time required, the samples were made as short as possible (**figure 3.6**) and large pressure differentials were applied. The sample dimensions were – 2.5cm (1") radius * 2mm (0.08") length. Upstream pressure was 13.8MPa (2000 psia) while downstream was left open to atmosphere.

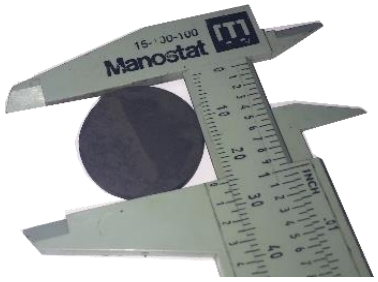

Figure 3.6: 2mm length Marcellus sample used for single phase brine permeability measurement at steady state flow conditions

3.1.5 Limitations of Approach

The mathematical formulation of the pulse decay permeability **equation 3-1** is based on the assumption of darcian flow or a viscous flow regime. However this assumption likely breaks down for tight rocks like shale. Darcian flow regimes exist when the Knudsen number (Kn) – the ratio between molecular mean-free-path to a characteristic length (pore radius for porous media) – is less than 0.01 (**Kuila et al. 2012**). While Knudsen number is not clearly defined for two-phase flow, (because of the absence of a clear definition of mean-free-path for two-phase flow) it will likely be large for rocks of small mean pore sizes. For such rocks like shale, with average pore sizes of under 100nm, it is possible that the knudsen number will be in the range of 0.01 to 10 and that a slip flow regime or a transitional flow regime towards full Knudsen diffusion (Kn > 10) exists. In such a scenario it becomes important to account for both darcian flow and Knudsen diffusion to accurately calculate rock permeability. This however, is not a trivial task when it comes to applications of two-phase flow such as relative permeability measurements.

An alternative to accounting for multiple flow regimes is to run experiments at high pressures, which reduce the molecular mean-free-path, thereby reducing Knudsen number. By running permeability experiments at multiple high pressures, one can extrapolate the data to infinite

pressure and compute permeability for a fully viscous flow regime. This approach was first suggested by **Klinkenberg, 1941** in order to correct for slip effects. However this approach was not considered practical for our applications because of the dynamic nature of two-phase permeability during continuous fluid imbibition.

Despite these limitations of the pulse decay-permeability technique, its application was still valid for our experiments because the objective was to observe relative changes in permeability over time. While accounting addition driving forces such as molecular diffusion for transport would certainly make our permeability calculations more robust, this would only serve to scale all the permeability measured for each individual sample by a constant amount without changing the general trends observed.

3.2 Materials Characterization

Keeping in mind the heterogeneities associated with shale formations, independent measurements were made to evaluate porosity, pore structure, and mineralogy. SEM imaging was used to make a qualitative visual assessment of porosity and pore connectivity. Millimeter size samples of rock were milled to $100\mu m * 30\mu m$ regions with focused ion beams of Gallium. Images were taken at several scales ranging from $50\mu m$ to $500nm$. X-Ray CT imaging was done at the beginning of each flow experiment to identify the presence of fracture channels.

Mercury injection porosimetry quantified effective porosity and pore size distribution in relatively rock chips weighing around 10gm and ~4cc. X-Ray diffraction analysis on crushed, powdered samples helped establish the mineralogy of the rocks.

4 Results and Discussion

4.1 Materials Characterization

4.1.1 Scanning Electron Microscopy (SEM)

The porosity in shales, as indicated by the dark black patches in **Figure 4.1** start to become clearly visible at magnifications of about 10k (**Figure 4.1 left**). However, zooming closer into the vicinity of large pores (**Figure 4.1 right**) indicates poor connectivity due to pore throats being very small and often filled with matter. Small pores appear to be disconnected in **Figure 4.2**. Even though true assessment of pore connectivity requires three-dimensional analysis, the SEM images suggest that a significant fraction of the matrix porosity of shales is disconnected. As such, isolated pores do not contribute to permeability at the scales of interest (core plug and larger).

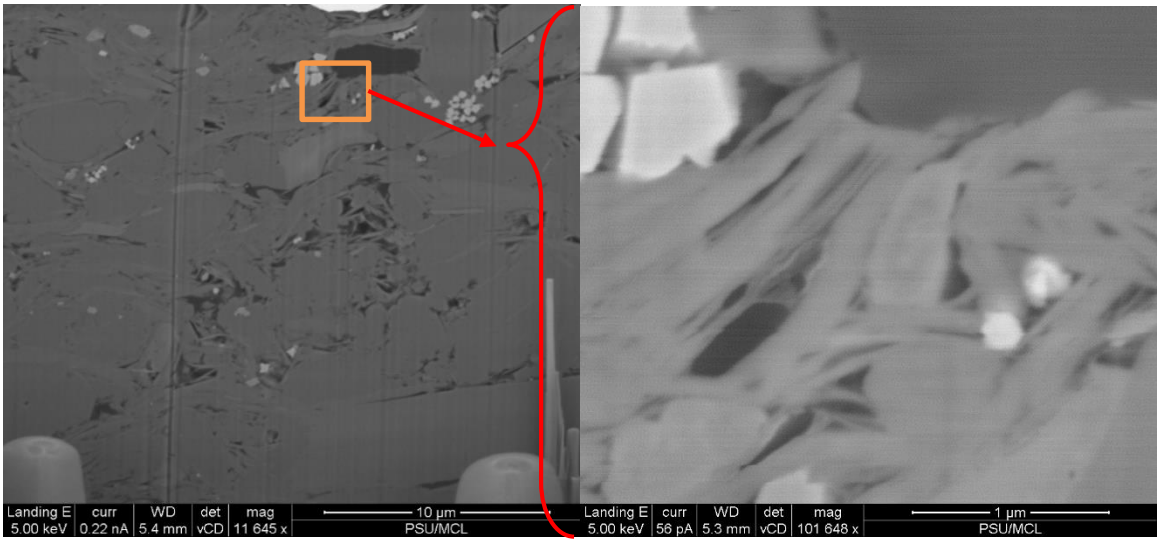

Figure 4.1: Left: SEM image showing porosity in a Marcellus shale sample

Right: Zoomed-in image of large pores showing filled pore throats

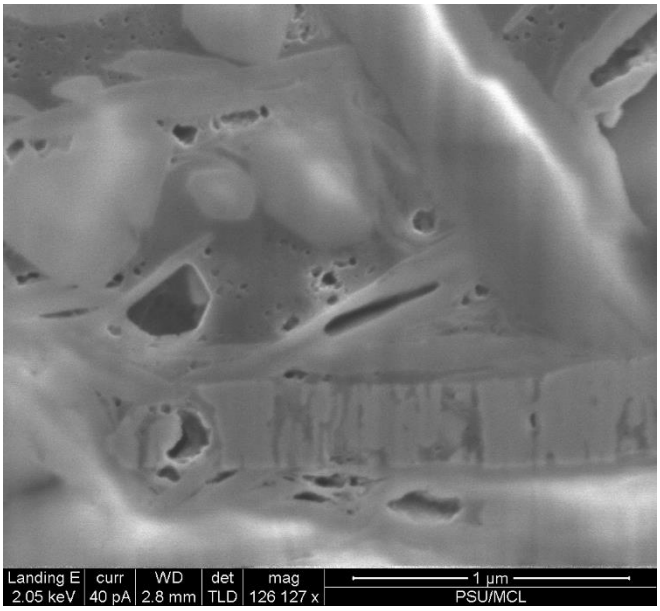

Figure 4.2: SEM image showing isolated organic content nano-pores in the Marcellus

4.1.2 X-Ray Diffraction

The results of X-Ray diffraction tests, **figure 4.3**, revealed Calcite, Quartz, Muscovite, Pyrite and clay minerals – particularly albite – to be the main constituent minerals for both rocks. However, only pyrite particles were distinctly visible as large white angular grains during SEM and X-ray CT imaging. Considering the moderate levels of clay content and apparent absence of swelling clays, it is possible that observations of permanent permeability damage from fluid leakoff by **Yan et. al. 2015** on Haynesville shale stems from the presence of these ultra-fine Calcite, Quartz and Muscovite particles mimicking clay effects, such as agglomeration, swelling and fine migration. This can also be a contributing factor to the declining permeability observed in this work (Section 4.2.2).

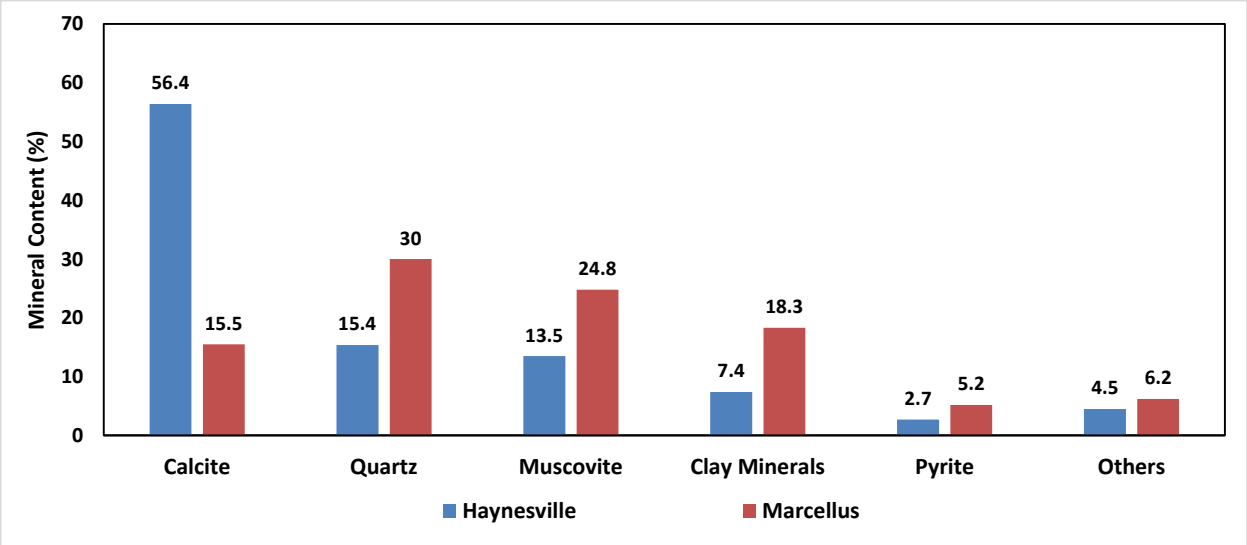

Figure 4.3: XRD Analysis showing mineralogical composition

4.1.3 Mercury Injection Porosimetry (MIP)

Mercury intrusion porosimetry is based on the principle that to force a non-wetting fluid into a capillary or pore of a certain diameter requires the application of a specific corresponding injection pressure. Thus the volume of mercury injected into a porous medium at every pressure step, starting at vacuum (3.5 kPa or 0.5psia) and gradually increasing pressure, gives an indication of the abundance of pores that have a diameter within a range that would see capillary instrusion for that pressure. In this way MIP can be used to measure pore size distribution of connected pores and also to measure effective porosity.

MIP porosity values were 3.2% and 1.5% for the Haynesville and Marcellus respectively. While these values are much lower than estimates found in the literature of Haynesville porosity at 8-14% **(Parker et. al. 2009)** and 10% for the Marcellus **(NETL 2011)**, they are in line with the qualitative estimates of porosity made during our flow experiments. Trends in pore size distribution **(Figure 4.4)** indicate that the higher Haynesville porosity may either be due to a bi-

modal distribution of micro and nano pores or due to the presence of a few anomalously large pores. Considering the high calcite content of the Haynesville, these are likely to be carbonate dissolution pores which are typically large and in most cases isolated. The Marcellus samples, on the other hand, appeared to have almost entirely nano scale porosity.

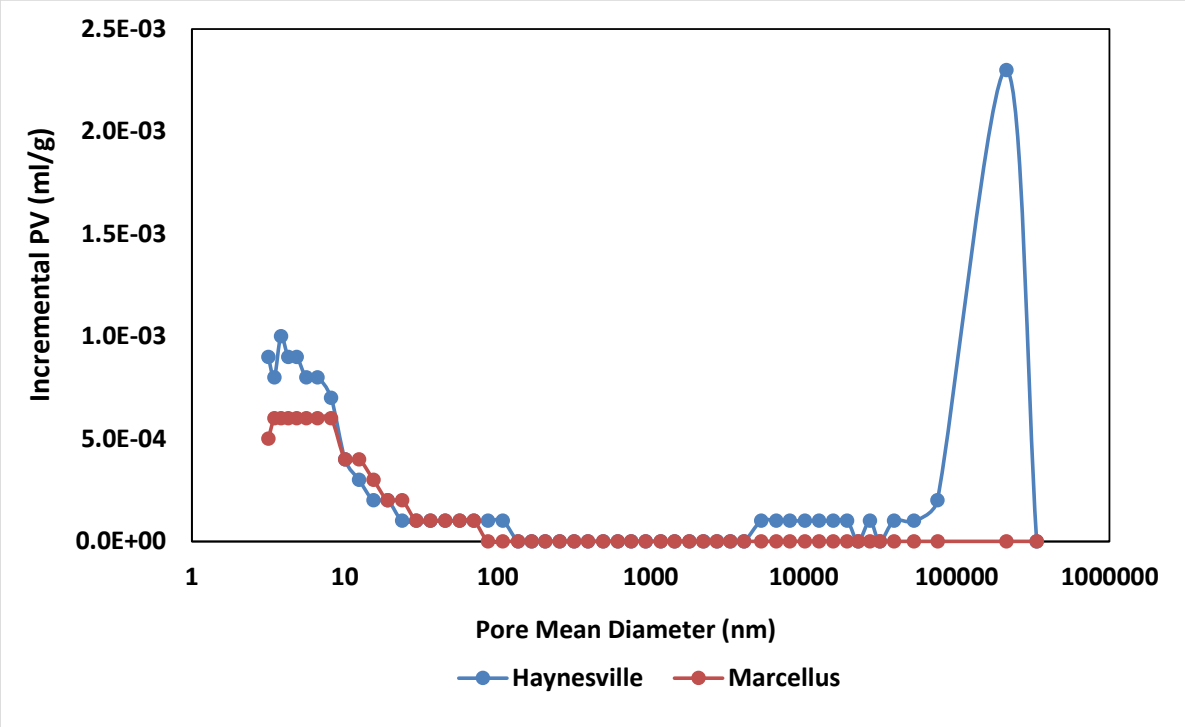

Figure 4.4: Pore Size distribution obtained from Mercury Porosimetry

In addition to porosity, mercury-air capillary pressure data was also obtained from MIP. These were then converted to water-air capillary pressure by using typical values of surface tension (λ)

and contact angle (θ) given in **table 4-1**. These yield a scaling factor of 0.05 when converting from mercury-air data to brine-argon using the **equation 4-1**.

$$Pc_{Brine-Argon} = Pc_{mercury-air} * \left(\frac{\lambda_{brine-argon}}{\lambda_{mercury-air}}\right) * \left(\frac{Cos\left(\theta_{brine-argon}\right)}{Cos\left(\theta_{mercury-air}\right)}\right)$$

Equation 4-1

Table 4-1: Surface tension and contact angle of fluid used for capillary pressure calculations

System	Contact Angle ($\boldsymbol{\theta}$)	Interfacial Tension ($\boldsymbol{\lambda}$)
Mercury-Air	140	485
Brine-Argon	105	70

The results (**figure 4.5**) indicate that at gas saturations as low as 40% for the Marcellus and 50% for the Haynesville, the brine-argon capillary pressures are greater than 6.9 Mpa (1000 psia). This might explain why return flow of brine water was not observed during flowback permeability measurements. This may also be a factor contributing to field observations of poor recovery of injected fracture fluids during flowback.

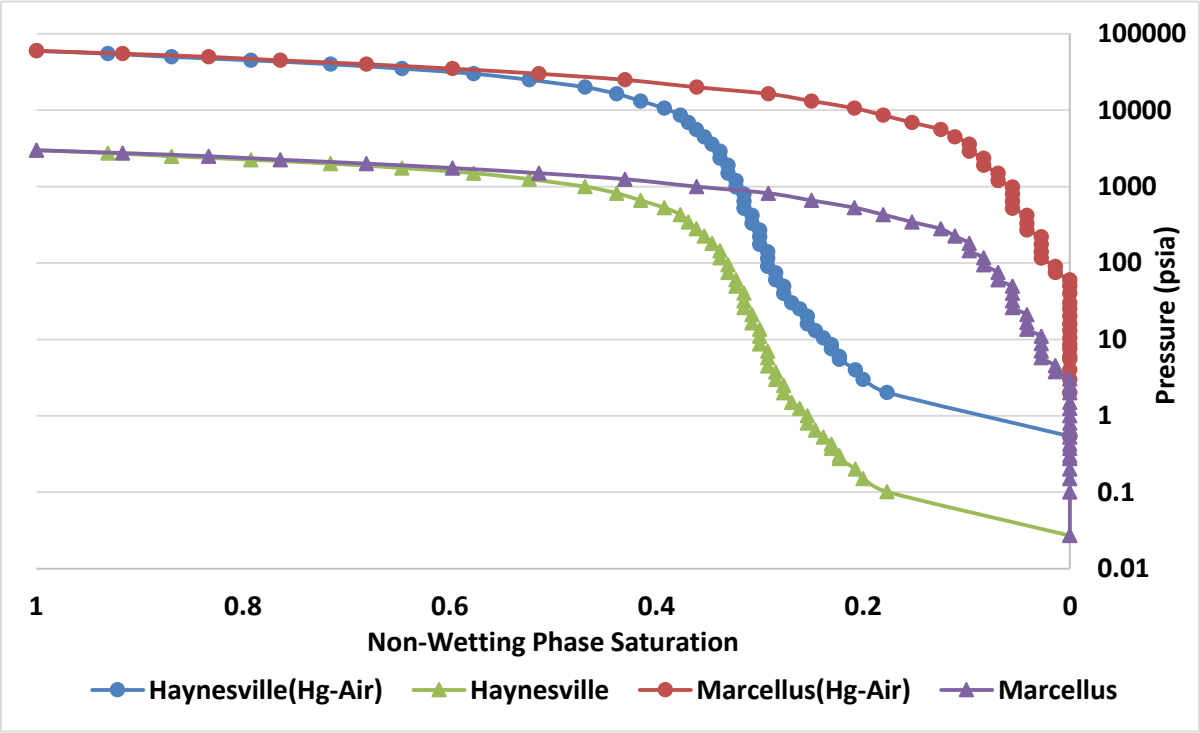

Figure 4.5: Capillary pressure curve derived from mercury porosimetry

4.2 Permeability evolution with soaking time

4.2.1 Base Permeability

The first step of soaking time vs permeability experiments was the establishment of dry matrix permeability to gas, referred to in this work as "base" permeability, shown in **Table 4-2**. These values vary widely across samples and show directional dependency relative to laminations and fractures introduced during sample preparation.

Table 4-2: Base Permeability and dimensions of core samples

Rock Type	Porosity (%)	Sample #	Orientation	Diameter cm	Length cm (inch)	Base Permeability nD
Marcellus	1.5	M1	Parallel	2.5 (1")	6.25 (2.5")	58.6
		M2	Parallel		4.75 (1.9")	19098 (19.1 µD)
		M3	Perpendicular		1.75 (0.7")	0.01 (qualitative)
		M4	Perpendicular		0.20 (0.08")	≤ 50
Haynesville	3.2	H1	Parallel		4.50 (1.8")	173

Most of the base permeabilities measured are "ultra-low", with values under 200nD. Sample M2 was the only outlier, with an exceptionally high reading of 19.1 µD. This was because it had a large transverse fracture running along the length of the core plug. The results of soaking time experiments, even on this sample, are still valuable because it is widely believed that most of the reservoir rock is naturally fractured in a similar fashion.

The results **(Table 4-2)** indicate marked differences between permeability measurements parallel and perpendicular to laminations in the Marcellus samples. The measured value perpendicular to lamination for sample M3 was below the limit of precision for the pulse decay apparatus (<<1nD). While single phase steady state flow through sample M4 yielded 50nD, although it must be pointed

out that the flow rate increased sharply at the end of the permeability measurement in sample M4, suggesting that the applied injection pressure had fractured the rock. Therefore, the original base permeability of M4 is likely to be significantly less than the reported 50nD. Experimental observations suggest that the higher parallel permeability measurements are largely due to flow through high-permeability streaks, such as fracture-like nano-channels existing along laminations, as can be seen in the X-ray CT image of the Haynesville sample H1 in **Figure 4.6**.

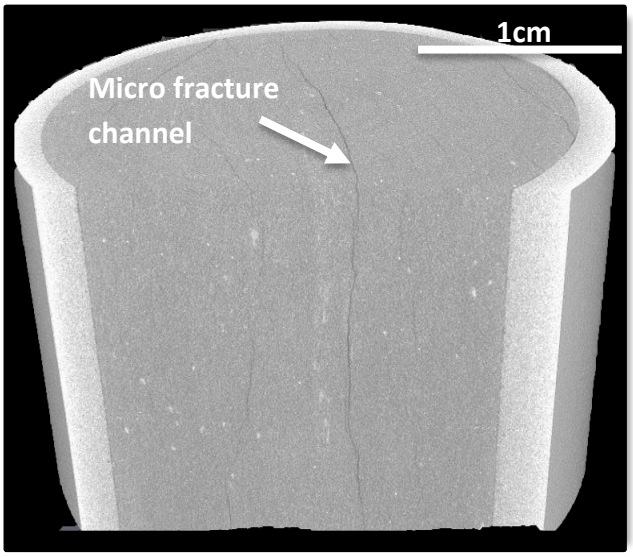

Figure 4.6: X-Ray CT image of the Haynesville sample H1 showing a distinct micro-fracture and other finer fractures running almost parallel to each other, all along the length of the sample

4.2.2 Soaking Time Permeability Evolution

Figure 4.7 shows the evolution of effective permeability to gas starting from leakoff and through soaking time experiments, with the y-axis representing permeability as a fraction (percentage) of base permeability. Damage to permeability due to initial leakoff fluid introduction, is represented by the first data point on each curve. This initial damage was most significant among ultra-tight samples M1, M2 and H1. Samples H1 and M1 lost 88% and 93% respectively of their base

permeability while the fractured M2 sample was affected even worse, losing 99% of its permeability, most likely because the choking of its main flow artery led to the permeability in M2 to drop closer to "true" matrix permeability levels. In contrast, the initial permeability loss was reported at around 70-80% for micro-Darcy range shale samples by **Yan et al. 2015** and only about 40-50% for milli-Darcy range tight sands by **Odumabo et al. 2014**.

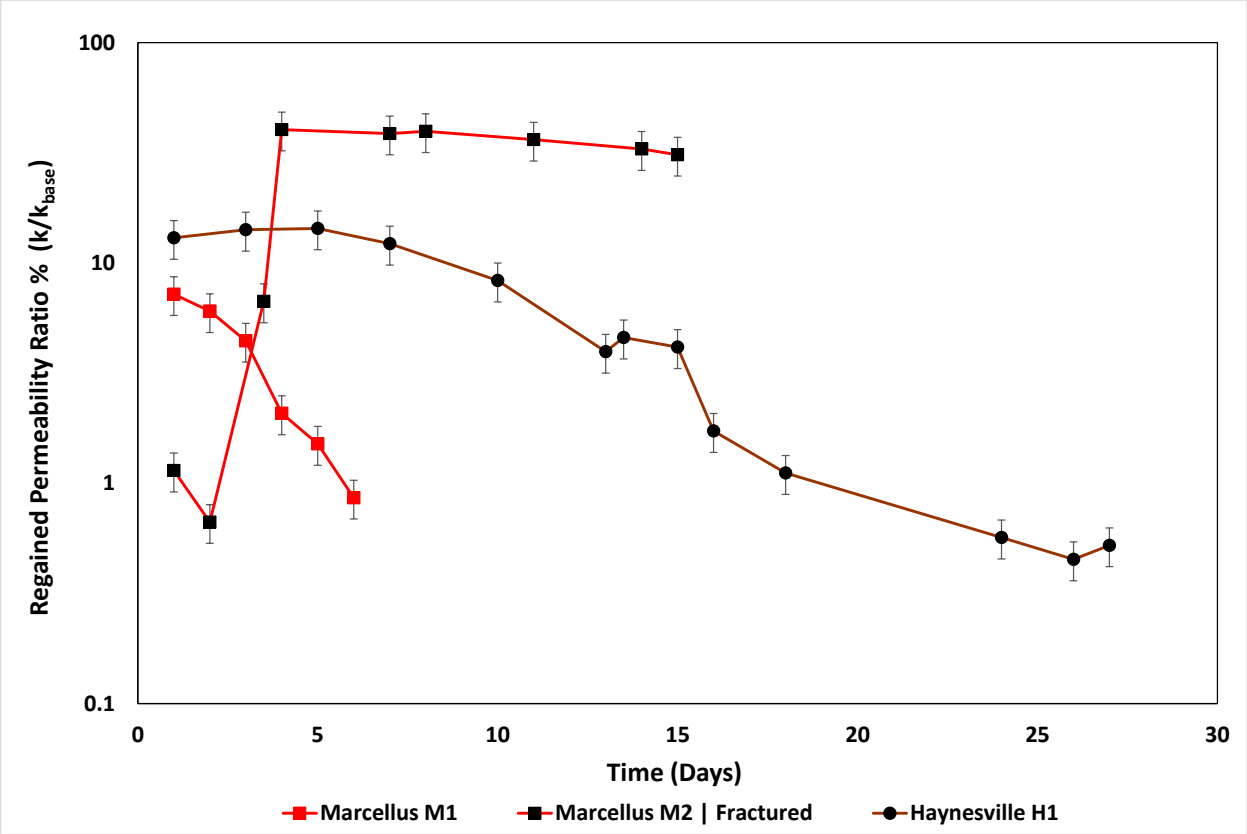

Figure 4.7: Shale permeability evolution with soaking time expressed as a ratio of measured effective permeability to base permeability. The estimated maximum error in measurement is +- 20% of the reported value.

Figure 4.8 is a compilation of data for these different rocks types with tight sand data from **Odumabo 2014**, medium permeability data from **Yan 2015**, and ultra-tight shale data from this work, represented on a Cartesian plot. While the first data point in all samples indicate damage due to leakoff, only the tight sands permeability of **Odumabo et al. 2014** show recovery with

soaking time. This Cartesian depiction is, however, insufficient to depict the orders of magnitude changes in shale permeability.

A broader perspective emerges from **Figure 4.9,** which is a semi-log representation of absolute effective permeability change with time, and strongly indicates that base permeability is a significant driver of permeability evolution. Samples with base permeability in the nano-Darcy range – H1 and M1 – saw significant reduction with time, each losing around 99.5% of base permeability by the end of the experiment. The rate of permeability reduction was also faster for the tighter Marcellus M1 sample. However, for samples with higher base permeability, soaking time has been found to be either inconsequential or beneficial. Recovery to up to 84% of base permeability was observed among tight sand samples by **Odumabo et al. 2014**.

This may be explained by one or more of the following reasons:

1. Capillary imbibition of liquid blocks is a function of mean size of the flow channels. In fractured shales ($k_g > 1\mu D$), the main permeability channels are the fractures. Therefore, when these channels are largely saturated with liquid, the permeability drops several orders of magnitude to true matrix levels. Capillary forces can help these fractures clear out fairly quickly during soaking time, thereby leading to significant recovery. This is the same process that leads to permeability recovery in the sands, with the difference that shale permeability is almost exclusively determined by fracture flow, instead of fracture and matrix.

2. In ultra-tight systems ($k < 500nD$), the flow channels – either nano-porosity or nano-fracture – are much smaller. This magnifies the scale of permeability damage caused by

the presence of liquids. Capillary imbibition forces are insufficient to overcome the inherently low permeability of these systems, and redistribution of fluid from liquid blocks is not as effective. The surface area of these nano flow channels is high, thus exacerbating effects such as clay swelling and particle agglomeration. This might explain the decline in permeability with soaking time and the irreversible damage to the base matrix permeability observed at the lab scale by **Yan et al. 2015.**

Another possible reason for these trends is that the redistribution of leakoff fluid during soaking time, results in growth of the liquid invaded zone. Two-phase gas relative permeability values, even at low water saturations, are extremely small in the case of ultra-tight shale reservoirs. Hence, a larger fluid invaded zone significantly enlarges the volume of the reservoir where gas is effectively immobile, thus lowering average permeability.

These results indicate that soaking time might be harmful to the long term productivity and ultimate recovery from shale formations. This observation may contradict the commonly held belief that soaking time is beneficial for gas production. Therefore, it is likely that the productivity increase seen in the field with post stimulation shut-ins comes from the drastic increase in fracture network connectivity induced by stimulation, while fluids clogging the fracture network are soaked up by the neighboring matrix. The fluid damage to matrix permeability may therefore be temporarily masked by the sudden increase in fracture connectivity. Moreover, studies of long term production such as **Crafton and Noe, 2013** of 270 shale wells, including 80 Marcellus wells**, s**how that soaking time may, in fact, be detrimental. The work presented in this paper provides supporting laboratory evidence for this observation.

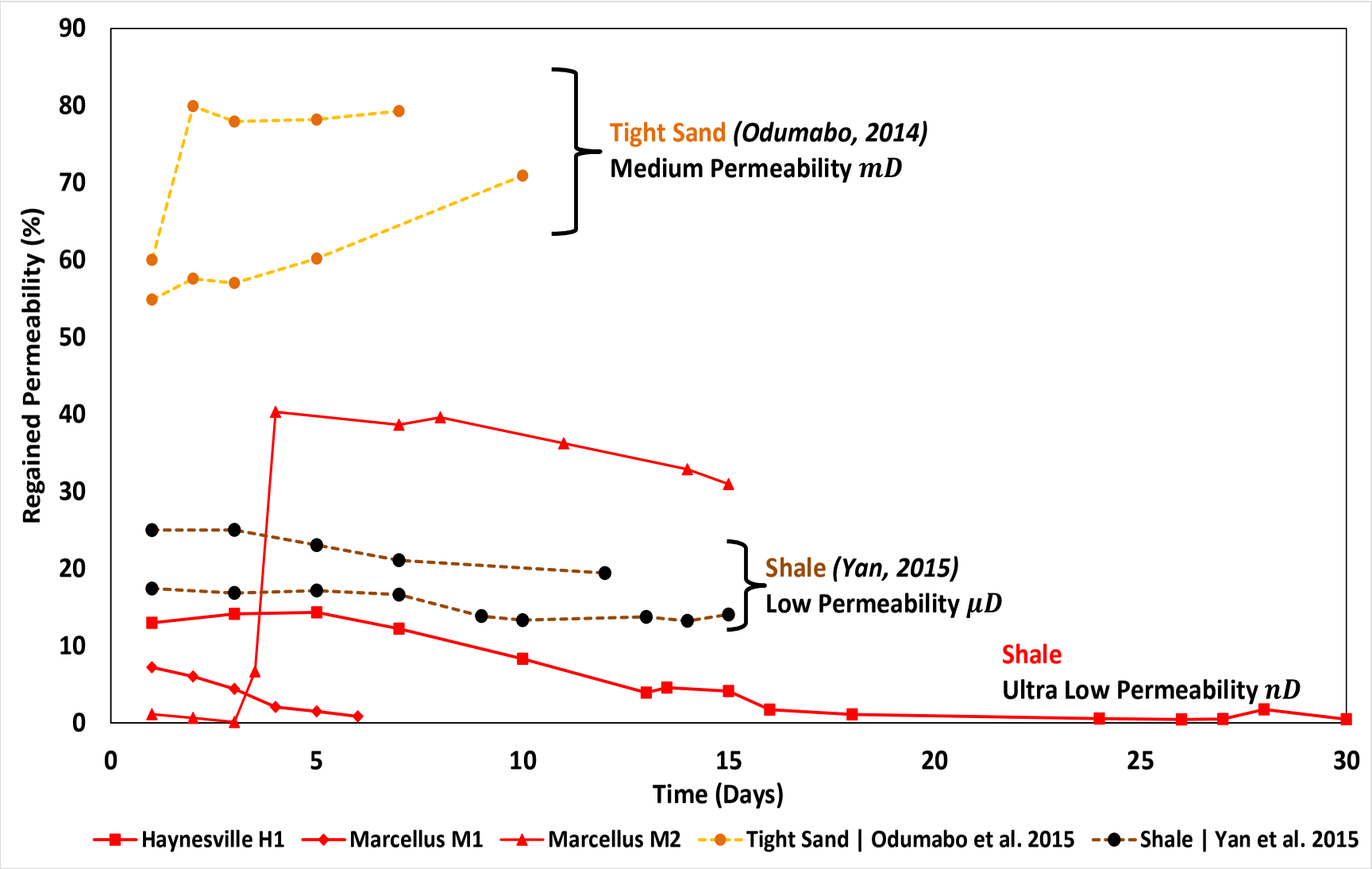

Figure 4.8: Cartesian Plot – Comparing tight sands, fractured shales and ultra-tight shale permeability evolution with soaking time. The first data point indicates leakoff damage in all cases. Permeability recovery with time is only observed with tight-sands and fractured shale.

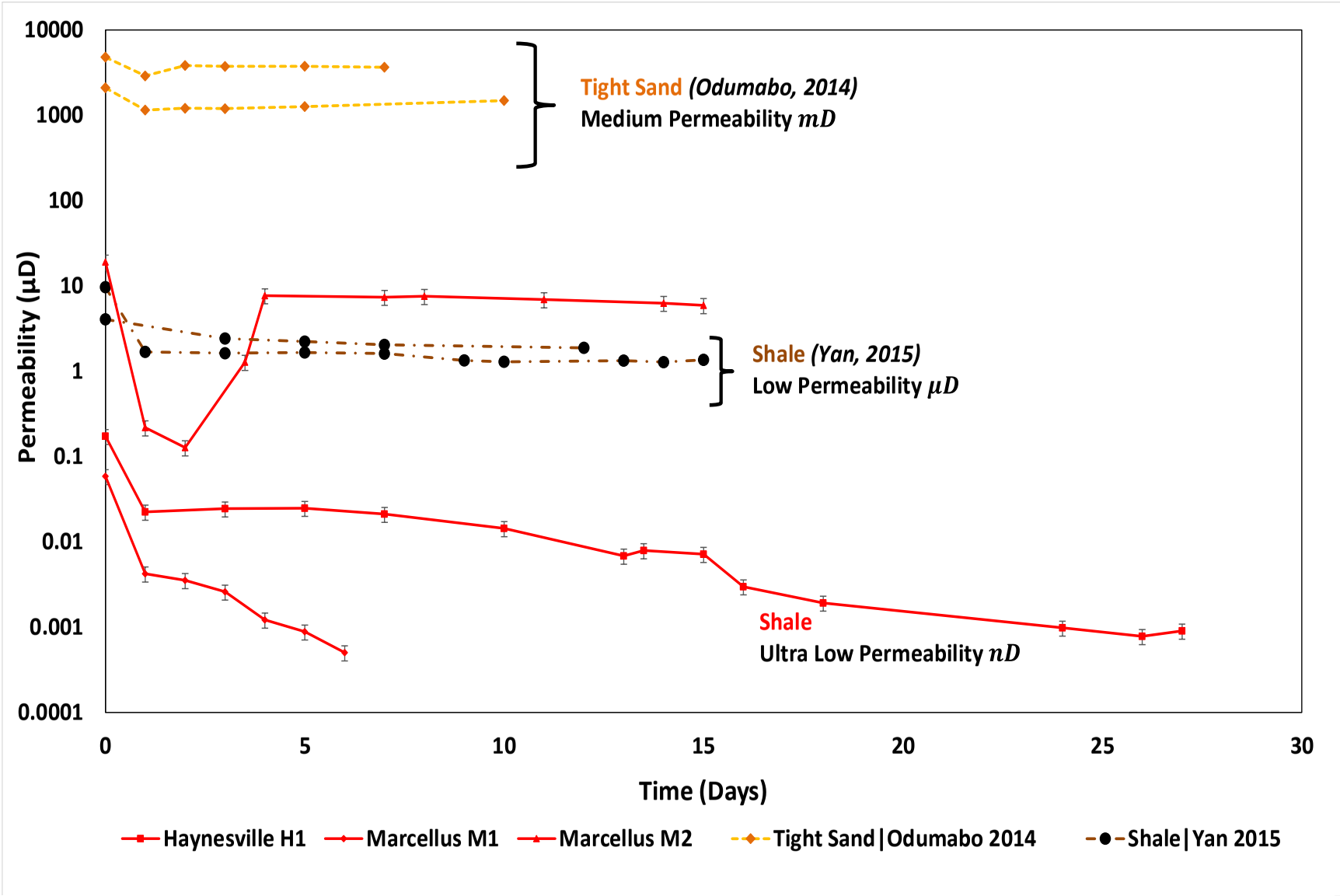

Figure 4.9: Semi-Log Plot: Comparing tight sands, fractured shales and ultra-tight shales. Permeability evolution with soaking time is a function of base permeability. Orders of magnitude permeability decline is observed in ultra-tight shale.

5 Conclusions

In this work, we have investigated the impact of soaking time on matrix permeability in ultra-tight shales through direct single-phase and two-phase gas permeability measurements. Detailed materials analysis including X-Ray CT, XRD, SEM, and Mercury Injection Porosimetry (MIP), have also been conducted to better explain the petrophysical characteristics observed.

The measurements of porosity and permeability were found to be highly sensitive to sample provenance, preparation and experimental conditions, and variations in measured values of permeability were in orders of magnitude. The results of this study indicate that ultra-tight shales have a large fraction of isolated pores and very low effective porosity. Matrix permeability in shales therefore appears to be strongly dependent on presence of laminations and associated nano-scale fracture channels. These channels may often be less than 1 micron wide and have significant tortuosity and therefore appear to be a part of the matrix porosity itself. The matrix also appears to be highly compartmentalized resulting in differences of 100 to 1000 times between permeability in the parallel and perpendicular lamination orientations. Laminations often manifest as micro-fractures arising out of the hydraulic and mechanical stimulation undergone by a sample during coring and preparation. Permeability measured parallel to lamination is in the range of tens of micro-Darcy (μD) for these fractured samples, significantly higher than intact samples whose permeabilities are in the nano-Darcy (nD) range.

Two-phase gas permeability measurements on partially water saturated samples reveal that permeability damage due to fluid leakoff is in the range of 90% to 99% in ultra-tight shales. Fluid imbibition with soaking time can further damage matrix permeability by up to 2 orders of magnitude. This is very different from the results of similar tests on tight sands and fractured

shales, indicating that evolution of permeability is a strong function of base permeability. The effects of soaking time become progressively less beneficial and more detrimental with tighter matrices.

This experimental analysis provides evidence that fluid flow through shales is significantly different from conventional rocks. This opens the door to more research on the true character of their flow network, and suggests keeping the role of laminations and micro-fractures at the heart of the investigation.

References

Bahrami, Hassan, Mohammad Reza Rezaee, Delair Honer Nazhat, Jakov Ostojic, Michael Benedict Clennell, and Ahmad Jamili. “Effect of Water Blocking Damage on Flow Efficiency and Productivity in Tight Gas Reservoirs.” Society of Petroleum Engineers, 2011. doi:10.2118/142283-MS.

Bhandari, Athma R., Peter B. Flemings, Peter J. Polito, Michael B. Cronin, and Steven L. Bryant. “Anisotropy and Stress Dependence of Permeability in the Barnett Shale.” *Transport in Porous Media* 108, no. 2 (March 8, 2015): 393–411. doi:10.1007/s11242-015-0482-0.

Bostrom, N., M. Chertov, M. Pagels, D. Willberg, A. Chertova, M. Davis, and W. Zagorski. “The Time-Dependent Permeability Damage Caused by Fracture Fluid.” In *SPE-168140-MS*. SPE: Society of Petroleum Engineers, 2014. doi:10.2118/168140-MS.

Britt, Larry Kevin, and Jerry Schoeffler. “The Geomechanics Of A Shale Play: What Makes A Shale Prospective.” Society of Petroleum Engineers, 2009. doi:10.2118/125525-MS.

Cantisano, Maria T., Dora P. Restrepo, Sandra Cespedes, Jonas Toelke, Avrami Grader, Michael Suhrer, and Joel Walls. “Relative Permeability in a Shale Formation in Colombia Using Digital Rock Physics,” 909–15. Society of Exploration Geophysicists, American Association of Petroleum Geologists, Society of Petroleum Engineers, 2013. doi:10.1190/urtec2013-092.

Cho, Younki, Erdal Ozkan, and Osman G. Apaydin. “Pressure-Dependent Natural-Fracture Permeability in Shale and Its Effect on Shale-Gas Well Production.” *SPE Reservoir Evaluation & Engineering* 16, no. 02 (May 1, 2013): 216–28. doi:10.2118/159801-PA.

Cipolla, Craig L., Elyezer P. Lolon, Jim C. Erdle, and Barry Rubin. “Reservoir Modeling in Shale-Gas Reservoirs.” *SPE Reservoir Evaluation & Engineering* 13, no. 04 (August 1, 2010): 638–53. doi:10.2118/125530-PA.

Cuisiat, Fabrice, Lars Grande, and Kaare Høeg. “Laboratory Testing Of Long Term Fracture Permeability In Shales.” Society of Petroleum Engineers, 2002. doi:10.2118/78215-MS.

Curtis, Mark Erman, Raymond Joseph Ambrose, Carl H. Sondergeld, and Chandra S. Rai. “Structural Characterization of Gas Shales on the Micro- and Nano-Scales.” Society of Petroleum Engineers, 2010. doi:10.2118/137693-MS.

Crafton, James, and Sandra Noe. “Impact of Delays and Shut-Ins on Well Productivity.” Society of Petroleum Engineers, 2013. doi:10.2118/165705-MS.

Daigle, Hugh, Sandra Ezidiegwu, and Raymond Turner. “Determining Relative Permeability In Shales By Including The Effects Of Pore Structure On Unsaturated Diffusion And Advection.” Society of Petroleum Engineers, 2015. doi:10.2118/175019-MS.

Energy Information Administration. 2015. Annual Energy Outlook – Early Release Overview, http://www.eia.gov/forecasts/aeo/pdf/0383(2014).pdf (downloaded 1 July 2015).

Glorioso, Juan Carlos, and Aquiles Jesus Rattia. “Unconventional Reservoirs: Basic Petrophysical Concepts for Shale Gas.” Society of Petroleum Engineers, 2012. doi:10.2118/153004-MS.

Gupta, Jugal, Elizabeth Templeton-Barrett, Yao Yao, Nancy Hyangsil Choi, Matias Zielonka, Heather Anne Burnham, Shalawn Jackson, Wadood El-Rabaa, and Richard Alan Albert. “Integration of Fracture, Reservoir, and Geomechanics Modeling for Shale Gas Reservoir Development.” Society of Petroleum Engineers, 2013. doi:10.2118/164018-MS.

Heller, Rob, John Vermylen, and Mark Zoback. “Experimental Investigation of Matrix Permeability of Gas Shales.” *AAPG Bulletin* 98, no. 5 (2014): 975–95. doi:10.1306/09231313023.

Holditch, Stephen A. “Factors Affecting Water Blocking and Gas Flow From Hydraulically Fractured Gas Wells.” *Journal of Petroleum Technology* 31, no. 12 (December 1, 1979): 1515–24. doi:10.2118/7561-PA.

Horsrud, P., E. F. SØnstebØ, and R. BØe. “Mechanical and Petrophysical Properties of North Sea Shales.” *International Journal of Rock Mechanics and Mining Sciences* 35, no. 8 (December 1998): 1009–20. doi:10.1016/S0148-9062(98)00162-4.

Jones, S.C. “A Technique for Faster Pulse-Decay Permeability Measurements in Tight Rocks.” *SPE Formation Evaluation* 12, no. 01 (March 1, 1997): 19–26. doi:10.2118/28450-PA.

Josh, M., L. Esteban, C. Delle Piane, J. Sarout, D. N. Dewhurst, and M. B. Clennell. “Laboratory Characterisation of Shale Properties.” *Journal of Petroleum Science and Engineering*, Unconventional hydrocarbons exploration and production Challenges, 88–89 (June 2012): 107–24. doi:10.1016/j.petrol.2012.01.023.

Katsube, T. J., Brett S. Mudford, and M. E. Best. “Petrophysical Characteristics of Shales from the Scotian Shelf.” *Geophysics* 56, no. 10 (October 1, 1991): 1681–89. doi:10.1190/1.1442980.

Klinkenberg, L. J. “The Permeability Of Porous Media To Liquids And Gases.” American Petroleum Institute, 1941.

Kovscek, Anthony R., and Arun Majumdar. *Natural Gas Resources, Natural Gas Utilization and Potential Climate/Pollution Benefits*. Vol. 1. 3 vols. Energy Seminar, Natural Gas Mini-

Series. Stanford: NVIDIA Auditorium, Jen-Hsun Huang Engineering Center, 2015. http://energyseminar.stanford.edu/node/637.

Kuila, Utpalendu, Manika Prasad, and Hossein Kazemi. “Application of Knudsen Flow in Modeling Gas-Flow in Shale Reservoirs,” 2012. http://www.spgindia.org/spg_2012/spgp182.pdf.

Landry, Christopher J., Adenike Tokan-Lawal, Masa Prodanovic, and Peter Eichhubl. “Matrix-Fracture Connectivity in Eagle Ford Shale.” American Association of Petroleum Geologists, 2014. doi:10.15530/urtec-2014-1922708.

Lan, Qing, Ebrahim Ghanbari, Hassan Dehghanpour, and Robert Hawkes. “Water Loss Versus Soaking Time: Spontaneous Imbibition in Tight Rocks.” *Energy Technology* 2, no. 12 (December 1, 2014): 1033–39. doi:10.1002/ente.201402039.

Li, Jun, Boyun Guo, Deli Gao, and Chi Ai. “The Effect of Fracture-Face Matrix Damage on Productivity of Fractures With Infinite and Finite Conductivities in Shale-Gas Reservoirs.” *SPE Drilling & Completion* 27, no. 03 (September 1, 2012): 348–54. doi:10.2118/143304-PA.

Neuzil, C. E. “How Permeable Are Clays and Shales?” *Water Resources Research* 30, no. 2 (February 1, 1994): 145–50. doi:10.1029/93WR02930.

Obaidy, Rawan T. I. Al-, Alain C Gringarten, and Vadim Sovetkin. “Modeling of Induced Hydraulically Fractured Wells in Shale Reservoirs Using ‘Branched’ Fractals.” Society of Petroleum Engineers, 2014. doi:10.2118/170822-MS.

Odumabo, S.M., Zuleima T. Karpyn, and Luis F. Ayala H. “Investigation of Gas Flow Hindrance due to Fracturing Fluid Leakoff in Low Permeability Sandstones.” *Journal of Natural Gas Science and Engineering* 17 (2014): 1–12. doi:10.1016/j.jngse.2013.12.002.

Olson, Karen, Alfred Daniel Hill, Kathryn Briggs, and Ding Zhu. “The Relationship between Rock Properties and Fracture Conductivity in the Fayetteville Shale.” Society of Petroleum Engineers, 2014. doi:10.2118/170790-MS.

Pagels, Markus, Dean M. Willberg, Eric Edelman, William Zagorski, and Joe Frantz. “Quantifying Fracturing Fluid Damage on Reservoir Rock to Optimize Production,” 1766–74. Society of Exploration Geophysicists, American Association of Petroleum Geologists, Society of Petroleum Engineers, 2013. doi:10.1190/urtec2013-180.

Roychaudhuri, Basabdatta, Theodore T. Tsotsis, and Kristian Jessen. “An Experimental and Numerical Investigation of Spontaneous Imbibition in Gas Shales.” Society of Petroleum Engineers, 2011. doi:10.2118/147652-MS.

Schieber, Juergen. “Common Themes in the Formation and Preservation of Intrinsic Porosity in Shales and Mudstones - Illustrated with Examples Across the Phanerozoic.” Society of Petroleum Engineers, 2010. doi:10.2118/132370-MS.

Tinni, Ali, Ebrahim Fathi, Rajiv Agarwal, Carl H. Sondergeld, I. Yucel Akkutlu, and Chandra Shekhar Rai. “Shale Permeability Measurements on Plugs and Crushed Samples.” Society of Petroleum Engineers, 2012. doi:10.2118/162235-MS.

Vega, Bolivia, Abhishek Dutta, and Anthony R. Kovscek. “CT Imaging of Low-Permeability, Dual-Porosity Systems Using High X-Ray Contrast Gas.” *Transport in Porous Media* 101, no. 1 (October 3, 2013): 81–97. doi:10.1007/s11242-013-0232-0.

Yan, Qiyan, Christina Lemanski, Zuleima T. Karpyn, and Luis F. Ayala H. “Experimental Investigation of Shale Gas Production Impairment due to Fracturing Fluid Migration during Shut-in Time.” *Journal of Natural Gas Science and Engineering* 24 (2015). doi:10.1016/j.jngse.2015.03.017.

Zhang, Junjing, Anton Kamenov, Alfred D. Hill, and Ding Zhu. “Laboratory Measurement of Hydraulic-Fracture Conductivities in the Barnett Shale.” *SPE Production & Operations* 29, no. 03 (August 1, 2014): 216–27. doi:10.2118/163839-PA.

Appendices

Appendix A: Core Holder Assembly

The core holder assembly housing the jacketed rock core sample and confining fluid is shown in **figure A.1**. The inner assembly of flowlines carrying brine and gas to the core sample are shown in **figure A.2**. The left hand side of the images is the downstream end from which brine injections were done. **Figure A.3** shows only the jacketed core plug connected to the flow distributors. **Figure A.4** shows the core sample extracted from the jacketing at the end of experiments. The jacketing is heat shrink polyolefin material that is designed to create an airtight seal around the core plug in order to prevent gas bypass during flowback permeability measurements. Therefore the jacketing had to be cut open in order to extract the sample. This extraction process caused some damages to the sample making it hard to get an accurate end point weight of intact liquid saturated core plug.

Figure A.1: Assembled Core Holder Setup

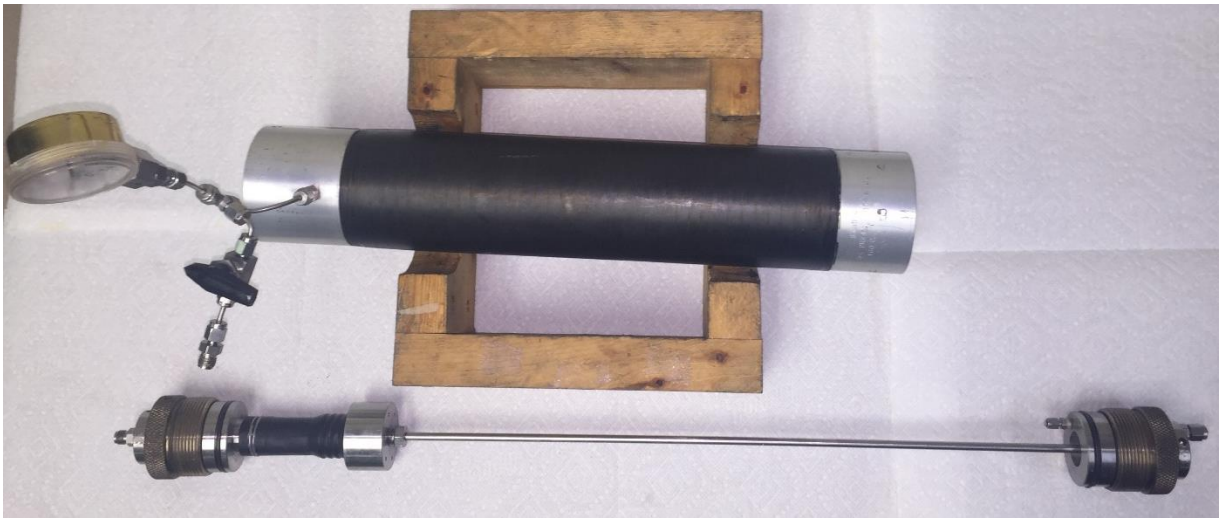

Figure A.2: Top: Core holder shell. Below: Inner axial flowline and jacketed core plug sample

Figure A.3: Core plug in black polyolefin jacketing attached to flow distributors

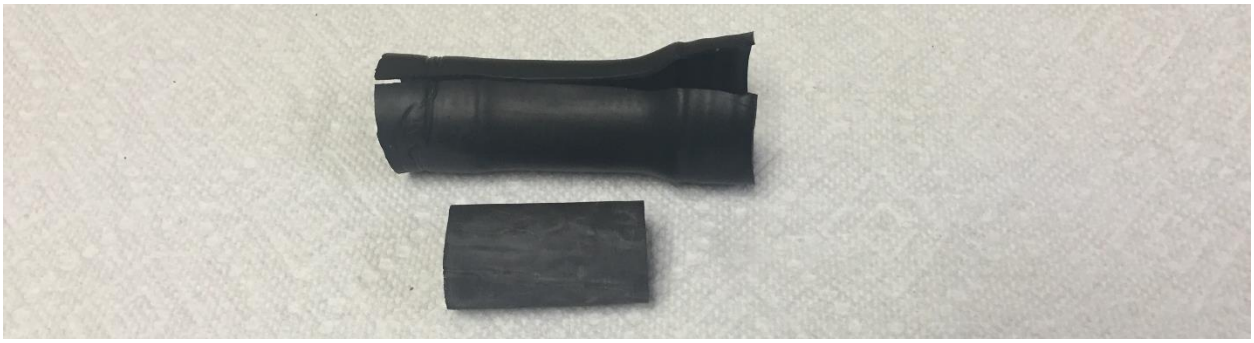

Figure A.4: Core plug sample extracted from jacketing at the end of an experiment

Appendix B: Permeability from Pressure Pulse Decay

The pulse decay permeability experiment is based on the assumption of linear one dimensional fluid flow through a core plug during a pulse decay or pressure pulse equilibration experiment. The diffusivity equation solved for one dimensional flow under transient conditions yields **equation B-1** which is an explicit equation to calculate permeability (**Jones, 1997)**.

$$k_g = \frac{-14696 m_1 \mu_g L f_z}{f_1 A p_m * \left(\frac{1}{V_1} + \frac{1}{V_2}\right)}$$

Equation 0-1

The results of a pulse decay experiments are logs of upstream and downstream pressure such as **figure B.1.**

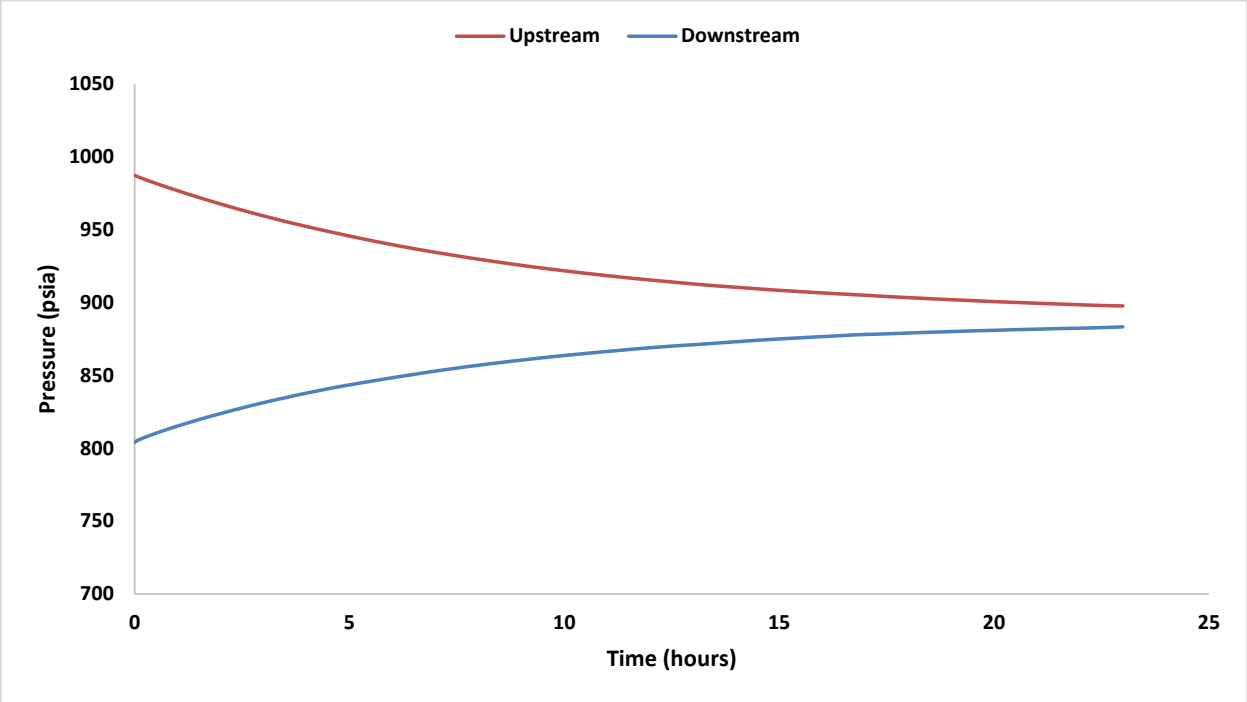

Figure B.1: Upstream and downstream pressure profile during a pulse decay permeability measurement that yielded 20nD permeabiliity

This pressure equilibration data is incorporated into **equation B-1** in the form of the coefficient m_1.

$\boldsymbol{m_1}$ *= slope of the logarithm of differential pressure vs time*

$$\ln[\Delta p] = b_1 + m_1 t$$

Equation B-2

where t is time in seconds

The differential pressure vs time semi-log plot, **figure B.2**, is constructed using the pressure profile data from the pulse decay experiments (**figure B.1**). It can be seen from the example in **figure B.2** that a straight line slope of differential pressure decline was observed right from the beginning of the experiment at pressure differential of 1.26 MPa (183 psi) until truncation at 0.1Mpa (15 psi). This fact was used to our advantage to make faster permeability measurements by using large pressure pulses wherein the initial decline rates are faster than for smaller pulses, and enabling us to use this initial data, thus obviating the need to wait until full pressure equilibrium.

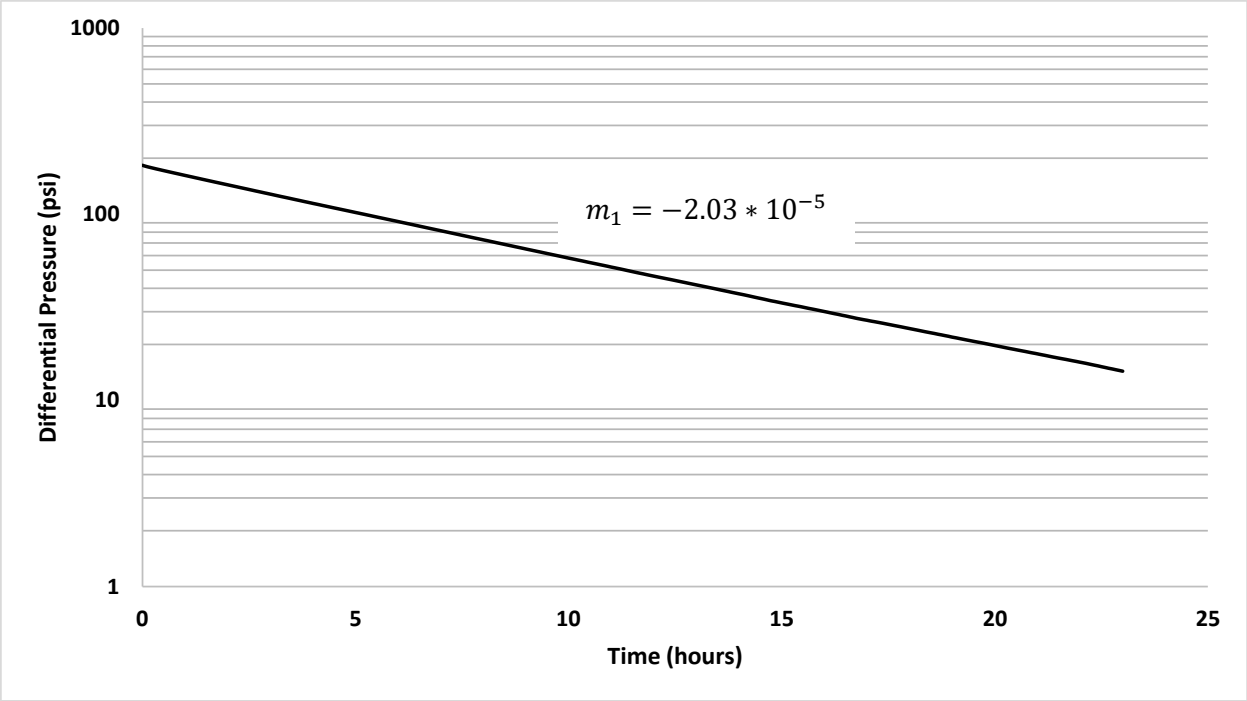

Figure B.2: Sample result from a pulse decay experiment that yielded a permeability of 20nD. To shorten the time taken to get a permeability reading, the experiment was truncated at a pressure difference of 15psia. Such truncations are possible because a clear straight line decline region was readily identifiable.

The remaining variables of **equation B-1** are described below.

Dimensional coefficients:

$\mathbf{A} = \text{cross} - \text{sectional area of cylindrical core plug, cm}^2$

$\mathbf{L} = \text{length of cylindrical core plug, cm}$

$\mathbf{V_1} = \text{Volume in small upstream reservoir, cm}^3$

$\mathbf{V_2} = \text{Volume in small downstream reservoir, cm}^3$

$\mathbf{p_m} = \text{mean pore pressure, psia}$

$\boldsymbol{\mu_g} = \text{viscosity of gas, cP}$

Dimensionless Coefficients:

$\boldsymbol{f_1} = mass\ flow\ correction\ factor$

The upstream and downstream volumes were designed to be almost equal to each other and therefore V2/V1 ratio assumed to be equal to 1. Depending on the core sample size, the ratio of pore volume to the pressure application volumes was between 0.25 to 0.65. The corresponding mass flow correction factor value to correct for this deviation from unity was obtained **table B-1** which has been sourced from **Jones, 1997**.

Table B-1: Values of f1 when V1/V2 close to 1 (Source: Jones, 1997)

	Values of f_1 for V_2/V_1=				
V_p/V_2	0.90	0.95	1.00	1.05	1.10
0.00	1.00000	1.00000	1.00000	1.00000	1.00000
0.05	0.99207	0.99191	0.99172	0.99150	0.99125
0.10	0.98424	0.98393	0.98355	0.98312	0.98263
0.15	0.97652	0.97605	0.97549	0.97485	0.97413
0.20	0.96889	0.96827	0.96754	0.96670	0.96575
0.25	0.96136	0.96060	0.95969	0.95865	0.95749
0.30	0.95393	0.95302	0.95194	0.95072	0.94935
0.35	0.94659	0.94554	0.94430	0.94289	0.94132
0.40	0.93935	0.93816	0.93676	0.93517	0.93340
0.45	0.93220	0.93087	0.92931	0.92755	0.92560
0.50	0.92514	0.92367	0.92196	0.92003	0.91790
0.55	0.91817	0.91657	0.91471	0.91262	0.91031
0.60	0.91129	0.90956	0.90755	0.90530	0.90283
0.65	0.90449	0.90264	0.90049	0.89808	0.89545
0.70	0.89778	0.89580	0.89352	0.89096	0.88817
0.75	0.89116	0.88905	0.88663	0.88394	0.88099
0.80	0.88462	0.88239	0.87984	0.87700	0.87391
0.85	0.87816	0.87581	0.87313	0.87016	0.86692
0.90	0.87178	0.86932	0.86651	0.86341	0.86004
0.95	0.86548	0.86290	0.85998	0.85675	0.85324
1.00	0.85925	0.85657	0.85353	0.85017	0.84654

$\boldsymbol{fz} = Gas\ compressibility\ Correction\ factor$

This factor accounts for deviations from ideal gas behavior and is important for pulse decay experiments run at high mean flowing pressures. This factor was calculated using pressure vs Z-factor values for Argon applied to **equation B-3**.

$$f_z = 1 - \frac{d\ln(z)}{d\ln(p)}$$

Equation B-3

The molar volume as a function of pressure and temperature (isothermal) was obtained from the National Institute of Standards and Technology (NIST) Webbook (webbook.nist.gov) and is given in **table B-2**. This was first used to compute Z factors as follows:

$$Z = \frac{pv_m}{RT}$$

Equation B-4

Thereafter, this was used to compute f_z.

$\boldsymbol{\mu_g} = Gas\ Viscosity$

Values of viscosity were also obtained from the NIST webbook[1] and are reported in **table B-2**. These may also be calculated in units of centi-poise using the Lee, Gonzales and Eakin Correlation. However it was found that the error due to calculation using empirical correlation may be as high as **20%.**

Table B-2: Argon Properties data obtained from NIST Web-book

Temperature (*R)	Pressure (psia)	Volume (ft3/lb-mole)	Z factor	Viscosity (cp)
531.6	754	7.3336	0.969402	0.023648
531.6	757.25	7.3013	0.969292	0.023655
531.6	760.5	7.2693	0.969186	0.023662
531.6	763.75	7.2376	0.969083	0.023668
531.6	767	7.2061	0.968971	0.023675
531.6	770.25	7.1749	0.968864	0.023682
531.6	773.5	7.1439	0.968748	0.023689
531.6	776.75	7.1132	0.968638	0.023696
531.6	780	7.0828	0.968534	0.023703
531.6	783.25	7.0526	0.968423	0.02371
531.6	786.5	7.0227	0.968318	0.023717
531.6	789.75	6.993	0.968208	0.023724
531.6	793	6.9636	0.968105	0.02373
531.6	796.25	6.9344	0.967996	0.023737
531.6	799.5	6.9054	0.967882	0.023744
531.6	802.75	6.8767	0.967778	0.023751
531.6	806	6.8482	0.967669	0.023758
531.6	809.25	6.82	0.96757	0.023765
531.6	812.5	6.7919	0.967453	0.023772
531.6	815.75	6.7641	0.967347	0.023779
531.6	819	6.7365	0.967238	0.023786
531.6	822.25	6.7092	0.967141	0.023793
531.6	825.5	6.682	0.967028	0.0238
531.6	828.75	6.6551	0.966926	0.023807
531.6	832	6.6284	0.966824	0.023814
531.6	835.25	6.6019	0.96672	0.023821
531.6	838.5	6.5756	0.966616	0.023829
531.6	841.75	6.5495	0.966511	0.023836
531.6	845	6.5236	0.966405	0.023843
531.6	848.25	6.4979	0.9663	0.02385
531.6	851.5	6.4724	0.966196	0.023857
531.6	854.75	6.4471	0.966093	0.023864
531.6	858	6.422	0.965991	0.023871
531.6	861.25	6.3971	0.96589	0.023878
531.6	864.5	6.3723	0.965776	0.023886
531.6	867.75	6.3478	0.96568	0.023893

Temperature (*R)	Pressure (psia)	Volume (ft3/lb-mole)	Z factor	Viscosity (cp)
531.6	1001	5.4796	0.961608	0.024196
531.6	1004.3	5.4614	0.961574	0.024204
531.6	1007.5	5.4432	0.961423	0.024211
531.6	1010.8	5.4252	0.961383	0.024219
531.6	1014	5.4073	0.961244	0.024227
531.6	1017.3	5.3895	0.961198	0.024234
531.6	1020.5	5.3718	0.961055	0.024242
531.6	1023.8	5.3542	0.961004	0.02425
531.6	1027	5.3367	0.960857	0.024257
531.6	1030.3	5.3194	0.960819	0.024265
531.6	1033.5	5.3022	0.960687	0.024273
531.6	1036.8	5.285	0.960628	0.02428
531.6	1040	5.268	0.960493	0.024288
531.6	1043.3	5.2511	0.96045	0.024296
531.6	1046.5	5.2343	0.960314	0.024304
531.6	1049.8	5.2176	0.960268	0.024311
531.6	1053	5.201	0.960131	0.024319
531.6	1056.3	5.1845	0.960085	0.024327
531.6	1059.5	5.1681	0.959947	0.024335
531.6	1062.8	5.1518	0.9599	0.024343
531.6	1066	5.1356	0.959762	0.02435
531.6	1069.3	5.1195	0.959715	0.024358
531.6	1072.5	5.1035	0.959579	0.024366
531.6	1075.8	5.0876	0.959533	0.024374
531.6	1079	5.0718	0.959398	0.024382
531.6	1082.3	5.0561	0.959353	0.02439
531.6	1085.5	5.0405	0.959221	0.024398
531.6	1088.8	5.025	0.959179	0.024405
531.6	1092	5.0096	0.959049	0.024413
531.6	1095.3	4.9942	0.958991	0.024421
531.6	1098.5	4.979	0.958865	0.024429
531.6	1101.8	4.9639	0.958829	0.024437
531.6	1105	4.9488	0.958688	0.024445
531.6	1108.3	4.9338	0.958637	0.024453
531.6	1111.5	4.919	0.958521	0.024461
531.6	1114.8	4.9042	0.958474	0.024469

531.6	871	6.3234	0.965571	0.0239
531.6	874.25	6.2992	0.965465	0.023907
531.6	877.5	6.2752	0.965362	0.023914
531.6	880.75	6.2514	0.965262	0.023922
531.6	884	6.2278	0.965166	0.023929
531.6	887.25	6.2043	0.96506	0.023936
531.6	890.5	6.181	0.964957	0.023943
531.6	893.75	6.1579	0.964859	0.023951
531.6	897	6.1349	0.964751	0.023958
531.6	900.25	6.1121	0.964648	0.023965
531.6	903.5	6.0895	0.964551	0.023972
531.6	906.75	6.0671	0.96446	0.02398
531.6	910	6.0448	0.964359	0.023987
531.6	913.25	6.0226	0.964249	0.023994
531.6	916.5	6.0006	0.964145	0.024002
531.6	919.75	5.9788	0.964049	0.024009
531.6	923	5.9571	0.963944	0.024016
531.6	926.25	5.9356	0.963847	0.024024
531.6	929.5	5.9143	0.963758	0.024031
531.6	932.75	5.893	0.963645	0.024038
531.6	936	5.872	0.963557	0.024046
531.6	939.25	5.8511	0.963461	0.024053
531.6	942.5	5.8303	0.963358	0.024061
531.6	945.75	5.8097	0.963264	0.024068
531.6	949	5.7892	0.963164	0.024076
531.6	952.25	5.7688	0.963057	0.024083
531.6	955.5	5.7486	0.96296	0.02409
531.6	958.75	5.7286	0.962873	0.024098
531.6	962	5.7086	0.962764	0.024105
531.6	965.25	5.6888	0.962666	0.024113
531.6	968.5	5.6692	0.96258	0.02412
531.6	971.75	5.6496	0.962471	0.024128
531.6	975	5.6302	0.962374	0.024135
531.6	978.25	5.611	0.962289	0.024143
531.6	981.5	5.5918	0.962182	0.02415
531.6	984.75	5.5728	0.962088	0.024158
531.6	988	5.5539	0.961989	0.024166

531.6	1118	4.8895	0.958344	0.024477
531.6	1121.3	4.8749	0.958303	0.024485
531.6	1124.5	4.8603	0.95816	0.024493
531.6	1127.8	4.8459	0.958124	0.024501
531.6	1131	4.8315	0.957988	0.024509
531.6	1134.3	4.8172	0.957939	0.024517
531.6	1137.5	4.803	0.95781	0.024525
531.6	1140.8	4.7889	0.957769	0.024533
531.6	1144	4.7749	0.957647	0.024541
531.6	1147.3	4.761	0.957614	0.024549
531.6	1150.5	4.7471	0.957481	0.024557
531.6	1153.8	4.7333	0.957436	0.024566
531.6	1157	4.7196	0.957313	0.024574
531.6	1160.3	4.7059	0.957256	0.024582
531.6	1163.5	4.6924	0.957143	0.02459
531.6	1166.8	4.6789	0.957096	0.024598
531.6	1170	4.6655	0.956972	0.024606
531.6	1173.3	4.6522	0.956936	0.024614
531.6	1176.5	4.6389	0.956802	0.024623
531.6	1179.8	4.6257	0.956756	0.024631
531.6	1183	4.6126	0.956634	0.024639
531.6	1186.3	4.5996	0.956599	0.024647
531.6	1189.5	4.5866	0.956468	0.024655
531.6	1192.8	4.5737	0.956424	0.024664
531.6	1196	4.5609	0.956306	0.024672
531.6	1199.3	4.5482	0.956275	0.02468
531.6	1202.5	4.5355	0.956149	0.024688
531.6	1205.8	4.5229	0.956109	0.024697
531.6	1209	4.5103	0.955976	0.024705
531.6	1212.3	4.4979	0.95595	0.024713
531.6	1215.5	4.4854	0.95581	0.024722
531.6	1218.8	4.4731	0.955777	0.02473
531.6	1222	4.4608	0.955651	0.024738
531.6	1225.3	4.4486	0.955611	0.024747
531.6	1228.5	4.4365	0.955501	0.024755
531.6	1231.8	4.4244	0.955454	0.024763
531.6	1235	4.4124	0.955338	0.024772

---

http://webbook.nist.gov/cgi/fluid.cgi?Action=Load&ID=C7440371&Type=IsoTherm&Digits=5&PLow=10&PHigh=2000&PInc=20&T=22&RefState=DEF&TUnit=C&PUnit=psia&DUnit=lbm%2Fft3&HUnit=Btu%2Flbm&WUnit=ft%2Fs&VisUnit=cP&STUnit=lb%2Fin

Appendix C: Computer Code for permeability calculation

The following is sample code for permeability calculation

```
%% Pulse Decay Permeability Calculation Code
%  by Nirjhor Chakraborty

clearvars
clc

%% Apparatus Inputs
d = 1; % core plug diameter in inches
L = 1.8; % length of core sample in inches
PV = pi*((0.5)^2)*L; % Bulk volume in inch^3
a=0.65; % Ratio of pore volume to pressure volumes V1 and/or V2 (Calculated
separately on a case by case basis)
V1 = 16.4*PV/a; % 1 in^3 = 16.4cm^3
V2 = 16.4*PV/a;
A = 6.45*pi*(d/2)^2; % Cross-sectional area of core plug in cm^2
f1 = 0.90; % Read off table B-1

%% Fluid Properties Data for Argon
Argon = xlsread('Data.xlsx','Argon','R3:T399'); % Properties given in table
B-2

p = Argon(:,1); % pressure in psia
z = Argon(:,2); % Z-factor
mu = Argon(:,3);% viscosity
lnp = log(Argon(:,1));
lnz = log(Argon(:,2));

n = length(z);

dlnz = diff(lnz);
dlnp = diff(lnp);

dlzlp = dlnz./dlnp;
fzvec = 1 - dlzlp;

%% Experiment Specific inputs

LOG = xlsread('Sample Pulse Decay.xlsx','Ex14nD','G2:N278'); % Data given in
table C-1

Pdn(:,1) = LOG(:,1); % Downstream Pressure in psia
Tdn(:,1) = LOG(:,2); % Downstream log temperature in centigrade (*C)
Pup(:,1) = LOG(:,4); % Downstream Pressure in psia
t(:,1) = LOG(:,8);   % time in seconds

T_C = mean(Tdn) ; % Average Temp in Centigrade
T = (T_C*(9/5) + 32) + 460; % Average Temp in Rankine
m = length(LOG);
```

```
Pm = (Pup(m) + Pdn(m))/2;
Z = interp1(p,z,Pm); % average Z-factor for flowing gas
fz = interp1(p(2:n),fzvec,Pm); % Gas compressibility correction factor
mum = interp1(p,mu,Pm); % Average viscosity of flowing gas

delp = Pup - Pdn; % Upstream and downstream pressure differential

semilogy(t,delp) % (Optional) semi-log plot of dP vs time - Used to confirm
straight line decline behavior

%% Slope Calculation

logdp = log(delp);
m1 = (log(delp(m)) - log(delp(1)))/(t(m) - t(1));

%% Permeability Calculation
kg = (-1469*m1*mum*(L*2.54)*fz)/(f1*A*Pm*( 1/V1 + 1/V2 ));
```

Table C-1: Sample log data from sample H1 yielding 20nD permeability

Downstream		Mean Pressure	Upstream		ΔP	ΔT
Pressure (psia)	Temperature (°C)	(psia)	Pressure (psia)	Temperature (°C)	(psia)	(sec)
804.1006	22.0688	895.6643	987.228	22.0632	183.1274	0
805.5142	22.1157	895.8726	986.231	22.1099	180.7168	300
806.572	22.1531	895.921	985.27	22.1477	178.698	600
807.5542	22.1819	895.953	984.3518	22.1787	176.7976	900
808.4858	22.208	895.9702	983.4546	22.2075	174.9688	1200
809.3838	22.231	895.9821	982.5803	22.2361	173.1965	1500
810.248	22.2512	895.9808	981.7136	22.2634	171.4656	1800
811.1213	22.2681	895.9954	980.8694	22.2876	169.7481	2100
811.9529	22.2856	895.9904	980.0278	22.3108	168.0749	2400
812.7664	22.3005	895.9838	979.2012	22.3337	166.4348	2700
813.5818	22.3135	895.9781	978.3743	22.3535	164.7925	3000
814.3933	22.3252	895.984	977.5747	22.3706	163.1814	3300
815.1746	22.3401	895.9678	976.761	22.3865	161.5864	3600
815.917	22.3533	895.9345	975.9519	22.4009	160.0349	3900
816.6689	22.3643	895.9001	975.1313	22.4133	158.4624	4200
817.417	22.3728	895.8802	974.3433	22.4238	156.9263	4500
818.1643	22.3838	895.8662	973.5681	22.4353	155.4038	4800
818.9075	22.3933	895.8529	972.7983	22.4478	153.8908	5100
819.6509	22.4043	895.8477	972.0444	22.459	152.3935	5400
820.3479	22.416	895.8133	971.2786	22.4697	150.9307	5700
821.041	22.4268	895.7816	970.5222	22.4788	149.4812	6000
821.7288	22.4351	895.7507	969.7725	22.4841	148.0437	6300
822.3945	22.4438	895.7149	969.0352	22.4949	146.6407	6600

823.0667	22.45	895.6895	968.3123	22.5037	145.2456	6900
823.709	22.4553	895.6416	967.5742	22.5127	143.8652	7200
824.3826	22.4609	895.6211	966.8596	22.5183	142.477	7500
825.0137	22.4653	895.5828	966.1519	22.5242	141.1382	7800
825.6931	22.4688	895.5759	965.4587	22.5317	139.7656	8100
826.333	22.4768	895.5476	964.7622	22.5386	138.4292	8400
826.9434	22.4839	895.504	964.0645	22.5437	137.1211	8700
827.5842	22.4895	895.4768	963.3694	22.5496	135.7852	9000
828.2234	22.4968	895.4635	962.7036	22.5544	134.4802	9300
828.8677	22.5042	895.4502	962.0327	22.5564	133.165	9600
829.436	22.5115	895.3993	961.3625	22.5601	131.9265	9900
830.0515	22.5159	895.3762	960.7009	22.5649	130.6494	10200
830.6394	22.5234	895.3518	960.0642	22.571	129.4248	10500
831.2212	22.5286	895.3253	959.4294	22.5818	128.2082	10800
831.8088	22.5327	895.2914	958.7739	22.5886	126.9651	11100
832.3921	22.5386	895.2679	958.1436	22.5891	125.7515	11400
832.9688	22.5464	895.2411	957.5134	22.5923	124.5446	11700
833.519	22.5537	895.2098	956.9006	22.5962	123.3816	12000
834.0359	22.5588	895.1541	956.2722	22.603	122.2363	12300
834.5586	22.5593	895.0948	955.6309	22.6086	121.0723	12600
835.1248	22.5588	895.0746	955.0244	22.6089	119.8996	12900
835.6506	22.561	895.0453	954.4399	22.6123	118.7893	13200
836.2217	22.5627	895.0435	953.8652	22.616	117.6435	13500
836.7656	22.5681	895.0316	953.2976	22.6179	116.532	13800
837.2737	22.5737	894.9927	952.7117	22.6233	115.438	14100
837.7874	22.5764	894.9581	952.1287	22.6287	114.3413	14400
838.2646	22.5801	894.9131	951.5615	22.6338	113.2969	14700
838.7627	22.5806	894.8789	950.9951	22.6409	112.2324	15000
839.2583	22.5815	894.8434	950.4285	22.6462	111.1702	15300
839.7478	22.584	894.8194	949.8909	22.6538	110.1431	15600
840.25	22.5869	894.8032	949.3564	22.6611	109.1064	15900
840.7427	22.5916	894.7825	948.8223	22.6702	108.0796	16200
841.2166	22.5972	894.7551	948.2935	22.6758	107.0769	16500
841.6812	22.6013	894.7234	947.7656	22.6812	106.0844	16800
842.1184	22.6045	894.6691	947.2197	22.6868	105.1013	17100
842.5508	22.6023	894.6133	946.6758	22.688	104.125	17400
842.9836	22.5969	894.5624	946.1411	22.6887	103.1575	17700
843.4136	22.5911	894.5089	945.6042	22.6882	102.1906	18000
843.8384	22.5854	894.4619	945.0854	22.6882	101.247	18300
844.2629	22.5796	894.418	944.573	22.6868	100.3101	18600
844.6794	22.5725	894.3671	944.0547	22.6865	99.3753	18900

845.0928	22.5662	894.3172	943.5415	22.6846	98.4487	19200
845.5105	22.5591	894.2721	943.0337	22.6829	97.5232	19500
845.9275	22.5537	894.2255	942.5234	22.6809	96.5959	19800
846.3379	22.5493	894.1877	942.0374	22.6792	95.6995	20100
846.7422	22.5442	894.149	941.5557	22.679	94.8135	20400
847.1479	22.54	894.1072	941.0664	22.6792	93.9185	20700
847.5464	22.5352	894.0697	940.593	22.6804	93.0466	21000
847.9446	22.5313	894.0375	940.1304	22.6809	92.1858	21300
848.3347	22.5286	893.994	939.6533	22.6809	91.3186	21600
848.7261	22.5254	893.9537	939.1812	22.6807	90.4551	21900
849.1084	22.5234	893.9148	938.7212	22.6792	89.6128	22200
849.4919	22.521	893.8903	938.2886	22.6787	88.7967	22500
849.8794	22.5181	893.8618	937.8442	22.6794	87.9648	22800
850.2625	22.5178	893.8252	937.3879	22.6812	87.1254	23100
850.6465	22.5193	893.7931	936.9397	22.6829	86.2932	23400
851.0205	22.5232	893.7594	936.4983	22.6841	85.4778	23700
851.4089	22.5271	893.7455	936.082	22.6848	84.6731	24000
851.793	22.5339	893.7256	935.6582	22.686	83.8652	24300
852.1545	22.54	893.6974	935.2402	22.688	83.0857	24600
852.5164	22.5459	893.6709	934.8254	22.6895	82.309	24900
852.8772	22.5498	893.648	934.4187	22.6919	81.5415	25200
853.2312	22.554	893.6193	934.0073	22.6953	80.7761	25500
853.5908	22.5574	893.5994	933.6079	22.6975	80.0171	25800
853.9429	22.5615	893.575	933.207	22.7007	79.2641	26100
854.2815	22.5662	893.5475	932.8135	22.7026	78.532	26400
854.6155	22.5703	893.5066	932.3977	22.7029	77.7822	26700
854.9492	22.5728	893.4738	931.9983	22.7004	77.0491	27000
855.2822	22.5762	893.4511	931.6199	22.6978	76.3377	27300
855.6089	22.5796	893.4182	931.2275	22.6973	75.6186	27600
855.9507	22.5813	893.3966	930.8425	22.6968	74.8918	27900
856.2688	22.5837	893.3679	930.467	22.6968	74.1982	28200
856.5801	22.5859	893.3374	930.0947	22.6965	73.5146	28500
856.8899	22.5876	893.3068	929.7236	22.697	72.8337	28800
857.197	22.5896	893.2794	929.3618	22.6973	72.1648	29100
857.509	22.593	893.2499	928.9907	22.6973	71.4817	29400
857.8228	22.5952	893.2236	928.6243	22.6953	70.8015	29700
858.135	22.5974	893.2011	928.2671	22.6936	70.1321	30000
858.427	22.5999	893.1703	927.9136	22.6951	69.4866	30300
858.7234	22.6013	893.1421	927.5608	22.6956	68.8374	30600
859.0144	22.6028	893.1092	927.2039	22.6953	68.1895	30900
859.3088	22.6042	893.0864	926.864	22.6958	67.5552	31200

859.5942	22.6045	893.0531	926.512	22.6956	66.9178	31500
859.8784	22.6062	893.0266	926.1748	22.6951	66.2964	31800
860.1572	22.6067	892.9954	925.8335	22.6951	65.6763	32100
860.4421	22.6084	892.9644	925.4866	22.6938	65.0445	32400
860.7205	22.6099	892.9394	925.1582	22.6917	64.4377	32700
860.9924	22.6116	892.9161	924.8398	22.6914	63.8474	33000
861.2625	22.6123	892.8886	924.5146	22.6914	63.2521	33300
861.5244	22.6143	892.8596	924.1948	22.6919	62.6704	33600
861.7964	22.6152	892.8371	923.8777	22.6917	62.0813	33900
862.0671	22.6169	892.8107	923.5542	22.6921	61.4871	34200
862.334	22.6191	892.7934	923.2527	22.6931	60.9187	34500
862.5916	22.6208	892.7718	922.9519	22.6936	60.3603	34800
862.8442	22.6213	892.7445	922.6448	22.6941	59.8006	35100
863.0923	22.6228	892.7155	922.3386	22.6951	59.2463	35400
863.3379	22.6216	892.6837	922.0295	22.697	58.6916	35700
863.5977	22.6211	892.663	921.7283	22.6968	58.1306	36000
863.8325	22.6216	892.6391	921.4456	22.6975	57.6131	36300
864.0742	22.6228	892.6159	921.1575	22.6992	57.0833	36600
864.3088	22.6233	892.5896	920.8704	22.7007	56.5616	36900
864.5388	22.6216	892.5636	920.5884	22.7021	56.0496	37200
864.7778	22.6213	892.5328	920.2878	22.7024	55.51	37500
865.0107	22.6213	892.5104	920.01	22.7009	54.9993	37800
865.2393	22.6228	892.4866	919.7339	22.7004	54.4946	38100
865.4634	22.623	892.4688	919.4741	22.7014	54.0107	38400
865.6912	22.6233	892.4467	919.2021	22.7029	53.5109	38700
865.916	22.6233	892.4275	918.939	22.7046	53.023	39000
866.1445	22.625	892.4085	918.6724	22.708	52.5279	39300
866.3757	22.6272	892.3849	918.394	22.7102	52.0183	39600
866.5908	22.6287	892.3677	918.1445	22.7102	51.5537	39900
866.8069	22.6309	892.3462	917.8855	22.7119	51.0786	40200
867.0205	22.6328	892.3266	917.6326	22.7139	50.6121	40500
867.2461	22.6348	892.3072	917.3682	22.7148	50.1221	40800
867.4666	22.6367	892.2836	917.1006	22.7148	49.634	41100
867.6921	22.6401	892.272	916.8518	22.7131	49.1597	41400
867.9094	22.6458	892.2562	916.603	22.7119	48.6936	41700
868.1157	22.6494	892.2359	916.356	22.7114	48.2403	42000
868.312	22.6519	892.2188	916.1255	22.7114	47.8135	42300
868.5195	22.6533	892.1997	915.8799	22.7117	47.3604	42600
868.7251	22.6555	892.1872	915.6492	22.7131	46.9241	42900
868.9182	22.6572	892.167	915.4158	22.7131	46.4976	43200
869.1062	22.6594	892.1463	915.1863	22.7146	46.0801	43500

869.2969	22.6606	892.13	914.9631	22.7173	45.6662	43800
869.4814	22.6611	892.1157	914.75	22.7209	45.2686	44100
869.6653	22.6614	892.0989	914.5325	22.7246	44.8672	44400
869.8447	22.6624	892.0781	914.3115	22.7292	44.4668	44700
870.0149	22.6609	892.0479	914.0808	22.7319	44.0659	45000
870.1841	22.6589	892.0174	913.8506	22.7354	43.6665	45300
870.3481	22.6553	891.984	913.6199	22.7373	43.2718	45600
870.5132	22.6509	891.9532	913.3931	22.7385	42.8799	45900
870.6824	22.6455	891.9248	913.1672	22.739	42.4848	46200
870.8413	22.6401	891.8925	912.9436	22.7393	42.1023	46500
871.0022	22.6343	891.8615	912.7207	22.7388	41.7185	46800
871.1665	22.6292	891.8394	912.5122	22.7368	41.3457	47100
871.324	22.6255	891.8079	912.2917	22.7349	40.9677	47400
871.4846	22.6213	891.7843	912.084	22.7336	40.5994	47700
871.6465	22.6169	891.7646	911.8826	22.7336	40.2361	48000
871.8032	22.6135	891.7407	911.6782	22.7334	39.875	48300
871.9902	22.6118	891.7347	911.4792	22.7336	39.489	48600
872.1909	22.6143	891.7506	911.3103	22.7334	39.1194	48900
872.3682	22.6179	891.7478	911.1274	22.7368	38.7592	49200
872.5391	22.6218	891.7431	910.947	22.7393	38.4079	49500
872.7195	22.6255	891.743	910.7664	22.7441	38.0469	49800
872.8796	22.6294	891.7327	910.5857	22.7493	37.7061	50100
873.0515	22.634	891.7337	910.4158	22.7546	37.3643	50400
873.2026	22.6389	891.7214	910.2402	22.76	37.0376	50700
873.3743	22.6438	891.7236	910.0728	22.7654	36.6985	51000
873.5479	22.6477	891.7173	909.8867	22.7676	36.3388	51300
873.7263	22.6548	891.7179	909.7095	22.7681	35.9832	51600
873.9036	22.6626	891.7209	909.5381	22.7695	35.6345	51900
874.0571	22.6699	891.7096	909.3621	22.771	35.305	52200
874.207	22.6743	891.6937	909.1804	22.7744	34.9734	52500
874.3745	22.6799	891.6917	909.0088	22.7754	34.6343	52800
874.5369	22.6853	891.6801	908.8232	22.7754	34.2863	53100
874.6541	22.6895	891.6579	908.6616	22.7749	34.0075	53400
874.7832	22.6909	891.636	908.4888	22.7771	33.7056	53700
874.9377	22.6912	891.6346	908.3315	22.7769	33.3938	54000
875.0833	22.6948	891.6329	908.1824	22.7783	33.0991	54300
875.2183	22.699	891.6259	908.0334	22.782	32.8151	54600
875.3677	22.7029	891.6264	907.885	22.7876	32.5173	54900
875.489	22.7075	891.6074	907.7258	22.7944	32.2368	55200
875.6079	22.7117	891.5952	907.5825	22.8022	31.9746	55500
875.7402	22.7119	891.5848	907.4294	22.811	31.6892	55800

875.8992	22.7156	891.5934	907.2876	22.8162	31.3884	56100
876.0381	22.718	891.5911	907.144	22.8176	31.1059	56400
876.1401	22.7197	891.5652	906.9902	22.8203	30.8501	56700
876.2837	22.7209	891.5696	906.8555	22.8254	30.5718	57000
876.4209	22.7227	891.5669	906.7129	22.8286	30.292	57300
876.5449	22.7251	891.5551	906.5652	22.8306	30.0203	57600
876.6704	22.7271	891.5454	906.4204	22.8306	29.75	57900
876.7981	22.7305	891.5326	906.2671	22.8306	29.469	58200
876.9233	22.7329	891.5261	906.1289	22.8311	29.2056	58500
877.0457	22.7366	891.5236	906.0015	22.8347	28.9558	58800
877.188	22.7402	891.5236	905.8591	22.8396	28.6711	59100
877.3308	22.7463	891.5441	905.7573	22.845	28.4265	59400
877.4727	22.7551	891.548	905.6233	22.8489	28.1506	59700
877.6038	22.7627	891.5497	905.4956	22.8506	27.8918	60000
877.7327	22.7698	891.5431	905.3535	22.854	27.6208	60300
877.8376	22.7764	891.5311	905.2246	22.8577	27.387	60600
877.9414	22.7815	891.5194	905.0974	22.8616	27.156	60900
878.0281	22.7815	891.5027	904.9773	22.8672	26.9492	61200
878.114	22.7813	891.4678	904.8215	22.8721	26.7075	61500
878.1746	22.7781	891.4279	904.6812	22.8728	26.5066	61800
878.2397	22.7698	891.3873	904.5349	22.8723	26.2952	62100
878.3069	22.7595	891.3452	904.3835	22.8704	26.0766	62400
878.3818	22.7512	891.3101	904.2383	22.8667	25.8565	62700
878.4707	22.7439	891.2844	904.0981	22.8628	25.6274	63000
878.5549	22.7378	891.2588	903.9626	22.8584	25.4077	63300
878.6448	22.7327	891.2378	903.8308	22.8562	25.186	63600
878.7363	22.7292	891.2255	903.7146	22.8545	24.9783	63900
878.8296	22.7288	891.2099	903.5901	22.8547	24.7605	64200
878.9287	22.7292	891.1959	903.4631	22.8557	24.5344	64500
879.0183	22.7307	891.1798	903.3413	22.8555	24.323	64800
879.1099	22.7324	891.1631	903.2163	22.8547	24.1064	65100
879.1997	22.7324	891.1488	903.0979	22.8547	23.8982	65400
879.2825	22.7322	891.1266	902.9707	22.8547	23.6882	65700
879.3772	22.7305	891.1129	902.8486	22.854	23.4714	66000
879.4556	22.7305	891.0896	902.7236	22.8525	23.268	66300
879.5356	22.7305	891.0719	902.6082	22.8506	23.0726	66600
879.6118	22.729	891.0534	902.4949	22.8494	22.8831	66900
879.6956	22.7271	891.0332	902.3708	22.8484	22.6752	67200
879.7693	22.7234	891.0126	902.2559	22.8469	22.4866	67500
879.8481	22.7214	890.9907	902.1333	22.8469	22.2852	67800
879.9343	22.72	890.9826	902.0308	22.8467	22.0965	68100

880.033	22.72	890.9712	901.9094	22.8469	21.8764	68400
880.1038	22.7214	890.9566	901.8093	22.8477	21.7055	68700
880.1882	22.7217	890.9428	901.6973	22.8484	21.5091	69000
880.2722	22.7227	890.9339	901.5955	22.8486	21.3233	69300
880.3469	22.7229	890.9138	901.4807	22.8486	21.1338	69600
880.4197	22.7229	890.8993	901.3789	22.8472	20.9592	69900
880.4854	22.7217	890.8725	901.2595	22.8467	20.7741	70200
880.5493	22.72	890.8501	901.1509	22.8455	20.6016	70500
880.6086	22.7161	890.825	901.0413	22.8435	20.4327	70800
880.6699	22.7122	890.8004	900.9309	22.843	20.261	71100
880.7388	22.7083	890.7808	900.8228	22.8413	20.084	71400
880.8081	22.7046	890.762	900.7158	22.8396	19.9077	71700
880.8789	22.7021	890.7431	900.6072	22.8374	19.7283	72000
880.9507	22.7004	890.729	900.5073	22.8357	19.5566	72300
881.0281	22.6992	890.719	900.4099	22.8347	19.3818	72600
881.1084	22.7007	890.7111	900.3137	22.8359	19.2053	72900
881.1895	22.7029	890.7077	900.2258	22.8364	19.0363	73200
881.2517	22.7046	890.6919	900.1321	22.8379	18.8804	73500
881.3228	22.7065	890.6825	900.0422	22.8379	18.7194	73800
881.3835	22.7078	890.6637	899.9438	22.8396	18.5603	74100
881.4431	22.7078	890.6475	899.8518	22.8398	18.4087	74400
881.5037	22.7065	890.6305	899.7573	22.8384	18.2536	74700
881.5598	22.7058	890.6024	899.645	22.8381	18.0852	75000
881.6116	22.7026	890.5823	899.553	22.8367	17.9414	75300
881.6711	22.7004	890.5663	899.4614	22.8362	17.7903	75600
881.7351	22.6992	890.5488	899.3625	22.8359	17.6274	75900
881.7976	22.699	890.5375	899.2773	22.8345	17.4797	76200
881.865	22.7004	890.5271	899.1892	22.8342	17.3242	76500
881.9338	22.7009	890.5162	899.0986	22.8342	17.1648	76800
882.0049	22.7036	890.5133	899.0217	22.8345	17.0168	77100
882.0645	22.7065	890.5031	898.9417	22.8345	16.8772	77400
882.1206	22.708	890.4909	898.8611	22.8362	16.7405	77700
882.1736	22.71	890.4785	898.7834	22.8364	16.6098	78000
882.2275	22.7085	890.4592	898.6909	22.8379	16.4634	78300
882.2751	22.7063	890.4365	898.5979	22.8364	16.3228	78600
882.3198	22.7043	890.414	898.5081	22.8347	16.1883	78900
882.366	22.7007	890.3885	898.4109	22.8325	16.0449	79200
882.4124	22.6965	890.3678	898.3232	22.8311	15.9108	79500
882.469	22.6934	890.3534	898.2378	22.8291	15.7688	79800
882.5283	22.6931	890.3378	898.1472	22.8271	15.6189	80100
882.6038	22.6934	890.3398	898.0757	22.8257	15.4719	80400

882.6692	22.6973	890.3388	898.0083	22.8286	15.3391	80700
882.7397	22.7026	890.3309	897.9221	22.8306	15.1824	81000
882.8091	22.7095	890.3308	897.8525	22.8303	15.0434	81300
882.9055	22.7163	890.3528	897.8	22.8308	14.8945	81600
882.989	22.7251	890.3718	897.7546	22.8347	14.7656	81900
883.0842	22.7332	890.398	897.7117	22.8435	14.6275	82200
883.1755	22.7437	890.4226	897.6697	22.8523	14.4942	82500
883.2588	22.7546	890.4369	897.615	22.8594	14.3562	82800